國立臺灣大學生命科學院生命科學系
碩士論文

Department of Life Science
College of Life Science
National Taiwan University
Master's Thesis

澤蛭 N teloblast 的轉錄體分析
Transcriptomic analysis of N teloblast in the leech *Helobdella austinensis*

李家容
Chia-Rong Li

指導教授：郭典翰 博士
Advisor: Dian-Han Kuo PhD

中華民國114年7月
July 2025

doi:10.6342/NTU202502160

國立臺灣大學碩士學位論文
口試委員會審定書
MASTER'S THESIS ACCEPTANCE CERTIFICATE
NATIONAL TAIWAN UNIVERSITY

澤蛭 *Helobdella austinensis* N teloblast 的轉錄體分析

Transcriptomic analysis of N teloblast in leech *Helobdella austinensis*

本論文係 李家容 R12B21011 在國立臺灣大學生命科學系完成之碩士學位論文，於民國 114 年 7 月 10 日承下列考試委員審查通過及口試及格，特此證明。

The undersigned, appointed by the Department of Life Science on 10th July 2025 have examined a Master's Thesis entitled above presented by Chia-Rong Li R12B21011 candidate and hereby certify that it is worthy of acceptance.

口試委員 Oral examination committee:

郭豐誠　張俊彥　游奇凱

（指導教授 Advisor）

系（所、學位學程）主管 Director: 鄭貽生

doi:10.6342/NTU202502160

致謝

兩年的碩士生涯即將於此劃下句點，在這兩年當中，我有所失去，也有所收穫。失去的是青春與熱血、是追求目標的強烈渴望、是奮不顧身的執著。失去固然讓人傷悲，但同時我也收穫了更加沉穩的自己。說白了，就是我摔斷腿打不了球，然後變胖。感謝我的小夥伴們在我最困難的時候向我伸出援手，照料我的生活起居。雖然偶爾會把我忘在系館，導致一整天沒吃到飯，但也是因為他們的呵護及陪伴，我才能再度投身於我的研究計畫。在二年級最忙碌的時候，也是這些小夥伴的存在，照亮了我最昏暗的幾個月。感謝你們願意幫我買飯、陪我做實驗到半夜、聽我訴苦，以及針對我的實驗給出建議，對我來說，你們是不可取代的一部分。

除此之外，還要感謝實驗室的兩位助理，帶我熟悉各個儀器的操作流程，並且指導我的研究方向。剛開始進入實驗室時，我就像一隻蒼蠅，在實驗室裡沒頭沒腦地亂飛，而那時助理們安排的教學實驗就像碩大無比的黏蒼蠅板，將我未來的命運和實驗室牢牢綑綁在一起。在共事的那段時間，助理們的研究經歷成為我之後實驗的墊腳石。儘管後來離職了，也會偶爾透過訊息關心我，提供我編寫論文的經驗。對我來說，助理們就像綠葉，不停地透過光合作用汲取養分，培養我這個初生新芽，而現在結出了果也算是不愧對他們的付出。

不論是綠葉還是新芽，都離不開背後默默支持的根。對實驗室而言，郭典翰老師就是我們的根。雖然老師人不狠、話也不多，像個慈眉善目的老父親，平時我做什麼實驗、什麼時間出現他一律不過問，但每當我實驗遇到瓶頸時，老師總是不遺餘力地提供支援。畢業在即，老師當年的一句話卻是言猶在耳：「能用錢解決的問題都是小問題。」這句話展現出老師深厚底蘊的同時，也透露出一絲霸道總裁般的魅力，收編了我的人，同時也收編了我的心。

最後，感謝我的家人。不論多辛苦，都笑著歡迎我回家；不論我做了什麼選擇，都全力支持。煽情的話等回家當面說，愛你們。

doi:10.6342/NTU202502160

中文摘要

細胞內物質的不對稱分離對澤蛭的早期胚胎發育至關重要。在卵裂過程中，一部分被稱為 teloplasm 的細胞質隨著細胞分裂分配至五對左右對稱的 teloblasts，決定其細胞類型。Teloblasts 進行多次幹細胞式不對稱分裂，產生一連串的初級胚母細胞 (primary blast cells)，進而發育為體節構造。胚胎學實驗顯示，N teloblasts 及初級胚母細胞的細胞命運並不需要細胞之間的交互作用，而是由細胞不對稱分裂自主調控產生，其分子機制仍不清楚。本研究首先對於 *Hau-EGL13a* 進行基因表現位置及功能性研究。*Hau-EGL13a* 是透過 EST-based 原位雜交染色檢測所發現、對 teloblast 具有專一性的基因，透過原位雜交染色，我發現該基因除了在 N teloblast 以外，還會表現在 M teloblast。以 Cas13d 對 N teloblast 進行 *Hau-EGL13a* knockdown 後並未造成可觀測的發育異常，表示該基因可能僅參與較為晚期的胚胎發育而非決定 N 細胞命運的決定因子。接著，我透過轉錄體分析找出在 N teloblasts 中有較高表現量的基因，並鑑定尋找可能影響 N teloblasts 命運的發育基因。而原位雜交染色顯示，在 N teloblasts 中表現較高的基因大多並非專一地表現在 N teloblasts，而是廣泛分布於各 teloblasts。Gene Ontology 分析顯示，在 N teloblasts 中高表現的基因主要與細胞生理活動相關，而非參與在胚胎發育或是細胞分化的過程。綜合而言，由母源 mRNA 不對稱分布所形成的細胞質決定物 (cytoplasmic determinant) 模型應該不是決定 N teloblasts 命運的機制。除了以 RNA 作為決定因子影響細胞命運外，透過蛋白質的不對稱分布引起區域性的轉譯調控同樣能在細胞分裂時使兩顆細胞產生不同的命運。參考上述模型，未來的研究方向應著重於蛋白質層面的分析，包含轉譯以及後轉錄修飾的調控。

關鍵字：胚胎發育、不對稱分裂、RNA 定序、轉錄體、Gene Ontology

doi:10.6342/NTU202502160

Abstract

Asymmetric segregation of cytoplasmic determinants plays a critical role in the early development of the leech. During cleavage, a pool of cytoplasm called teloplasm segregates into five bilateral pairs of teloblasts to specify teloblast identities. A teloblast then undergoes iterated stem-cell-like asymmetric divisions to produce a bandlet of primary blast cells, or segment founder cells, each gives rise to a set of serially homologous progeny. Among the five teloblast pairs, the N teloblast mainly contributes to the central nervous system. Embryological experiments revealed that, fate specification of N teloblasts and primary blast cells is cell autonomous. However, molecular identities for the determinants of teloblasts and primary blast cells remain elusive. In this study, I first investigated the expression pattern and function of Hau-EGL13a, a teloblast-specific gene identified through an EST-based in situ hybridization screen. Although initially detected in the N teloblast, Hau-EGL13a was also expressed in the M teloblast. Cas13d-mediated knockdown of Hau-EGL13a in the N teloblast did not result in observable phenotypic changes, suggesting that it functions as a regulator of later developmental processes in teloblasts rather than serving as a determinant of initial cell fate. Subsequently, I performed transcriptome analysis to identify potential RNA determinants of N fate by searching for transcripts enriched in N teloblasts. Unexpectedly, most statistically significant candidates are only slightly enriched in N teloblast. In situ hybridization analysis showed that they are broadly distributed and not specifically localized to the N teloblast. GO analysis indicated that these N-enriched genes are most related to metabolic process, and are not associated with embryonic development or cell differentiation. Together, our results suggest that the molecular mechanism for the specification of N teloblast does not follow the

doi:10.6342/NTU202502160

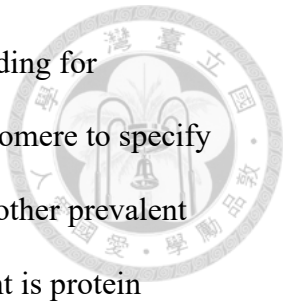

standard model of cytoplasmic determinant in which transcripts encoding for developmental regulatory genes is specifically segregated into a blastomere to specify its developmental fate. In addition to the RNA segregation model, another prevalent mechanism for specifying cell identity during embryonic development is protein localization, which is commonly observed across diverse species. Accordingly, future research should focus on protein-level processes, including translational control and transcriptional regulation.

Keywords: Embryonic development, Asymmetric division, RNA sequencing, Transcriptome, Gene ontology.

doi:10.6342/NTU202502160

Table of Contents

doi:10.6342/NTU202502160

doi:10.6342/NTU202502160

List of Figures

doi:10.6342/NTU202502160

doi:10.6342/NTU202502160

List of Tables

doi:10.6342/NTU202502160

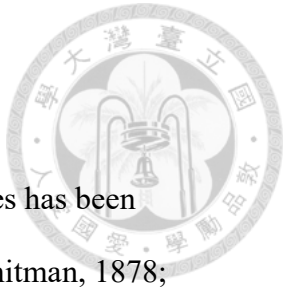

Introduction

Historically, the embryonic development of glossiphoniid leeches has been extensively studied in terms of cell lineage since the 19th century (Whitman, 1878; 1887). Similar to embryos of other spiralian phyla, their embryos undergo spiral cleavage, a process characterized by a 45° shift in the mitotic spindle relative to the animal-vegetal axis from the third cleavage and onward (Meshcheryakov & Beloussov, 1975; Martín-Durán & Marlétaz, 2020). Spiral cleavage involves asymmetric cell division and differential segregation of cell contents, resulting in a size difference between sister blastomeres, and therefore, every cell in an embryo with the spiral cleavage pattern can be uniquely identified by its size and position. Furthermore, this feature also permits a direct comparison of embryonic development across phyla. It was found that the developmental fates of these identified blastomeres are often conserved across phyla, making them a useful model for studying the evolutionary diversification of animal body plans (Henry, 2014).

Nevertheless, the spiral cleavage of the leech and oligochaete embryo has been modified as an adaptive evolutionary change for invading the freshwater and terrestrial habitats in this annelid lineage (Kuo, 2017). Specifically, the differences in the timing and the degree of asymmetry of cell divisions between different lineages have become more exaggerated in the leech compared to the ancestral condition observed in the marine polychaete annelids. Further, the developmental patterning has become increasingly cell-lineage driven. No true “embryonic organizer” – a cell population responsible for patterning the axial organization of the entire embryo – was ever found in oligochaetes and leeches (Nakamoto et al., 2011). In contrast, a D quadrant organizer is responsible for dorsoventral patterning in polychaete annelids (Seudre et al., 2022).

doi:10.6342/NTU202502160

Therefore, comparing the molecular mechanism of cell lineage-dependent axial patterning in leech embryogenesis with axial patterning mechanisms in polychaetes may help to understand the evolutionary emergence of embryonic cell lineage stereotypy, which is also observed in ascidian and nematode embryos.

Given the significant morphological difference between the leech and polychaete embryos, a specialized nomenclature, informed by knowledge of prospective cell fates in the embryo, has been established for the leeches (Bissen & Weisblat, 1989; Fernández & Stent, 1980; Weisblat & Huang, 2001; Huang et al., 2002). In this nomenclature system, the four large cells arising from the first two divisions are designated as macromeres A, B, C, and D. These macromeres can be distinguished by their size and arrangement. Viewed from the animal pole, macromeres A, B, C, and D are arranged in a clockwise pattern, with macromere D being noticeably larger than other macromeres (Figure 1, stage 1-3).

Macromere D then divides into a macromere (D') and a micromere (d') (Figure 1, stage 4). Macromere D' then further divides into the mesodermal progenitor, DM, at the vegetal pole and the ectodermal progenitor, DNOPQ, at the animal pole. DM divides into teloblasts M_L and M_R, contributing to the mesodermal parts such as muscles and nephridia (Zackson, 1982; Weisblat and Shankland, 1985; Gline et al., 2011). Meanwhile, DNOPQ divides into $NOPQ_L$ and $NOPQ_R$, and each of them then sequentially generates an N, a Q, and finally two developmentally equivalent O/P teloblasts. These four pairs of DNOPQ-derived teloblasts are ectoteloblasts because they eventually give rise to ectodermal tissues such as the nervous system and epithelium (Weisblat et al., 1978; Weisblat and Shankland, 1985).

Each teloblast undergoes repeated rounds of highly asymmetric divisions in quick succession to produce a sequential series of primary blast cells, forming a band-like

doi:10.6342/NTU202502160

structure called a bandlet (Zackson, 1982; 1984). All of these bandlets contribute to the bilaterally symmetric germinal bands (Figure 1, stage 7-8). As the embryonic development proceeds, the germinal bands elongate and migrate across from the dorsal aspect of the embryo toward the prospective ventral midline in the process of epiboly gastrulation (Smith et al., 1996). Eventually, the left and right germinal bands fuse at the ventral midline to form the germinal plate and thus complete the gastrulation.

Leeches are annelids, whose body plan is characterized by having a segmented trunk and a non-segmental prostomium (or head). Leech segmentation is coupled to the production of primary blast cells and thus the division of teloblasts. In the M, O, and P lineages, each segment is composed of a progeny derived from a single primary blast cell. In contrast, the N and Q lineages generate two distinct types of primary blast cells, nf and ns in the N lineage or qf and qs in the Q lineage, in an alternating pattern (Zackson, 1982; 1984). As a result, each segment in the N and Q lineages is formed by the progenies derived from two different primary blast cells, whereas it is derived from a single primary blast cell in the O, P, and M lineages (Weisblat and Shankland, 1985) (Figure 2).

In the N teloblast lineage, the primary blast cells (nf and ns) divides to produce the secondary blast cells (nf.a, nf.p, ns.a, and ns.p, so named to denote their progenitor origin and relative anterior-posterior positioning). The anterior nf.a is notably larger than the posterior nf.p, whereas ns.a and ns.p are similar in size. These secondary blast cells subsequently divide multiple times, giving rise to neural progenitors, which contribute to segmental ganglia development along the anterior-posterior axis in a stepwise manner (Martindale & Shankland, 1990). Moreover, cell ablation experiments in the N lineage suggest that blast cell identity within the n-lineage is autonomously specified (Bissen & Weisblat, 1987; Ramirez, 1995; Shain et al., 2000). As is in major

doi:10.6342/NTU202502160

paradigms of cell autonomous specification, it was thought that this unique behavior is specified by differential inheritance of cell intrinsic factors such as cytoplasmic determinants by the N teloblast. A similar mechanism may also be responsible for the specification of nf and ns fates among the primary blast cells (Zhang et al., 2009).

A major candidate for such cytoplasmic determinants is localized mRNA, as asymmetric segregation of RNA during embryonic development has been observed across different animal taxa, including molluscs (Lambert & Nagy, 2002; Henry et al., 2010), arthropods (Knoblich, 2008; Lasko, 2012), and mammals (Shlyakhtina, 2019). Further, in the ascidian embryo, which has a stereotyped cell lineage similar to the leech, muscle cell fate is shown to have been determined by inheritance of RNA cytoplasmic determinants (Nishida and Sawada, 2001).

In the leech embryo, teloplasm has long been considered to embody the cytoplasmic determinant for teloblast fates (Weisblat & Kuo, 2014). This idea is supported by the cytoplasm redistribution experiments showing that inheritance of teloplasm is both sufficient and required for specifying the blastomere identity of teloblast progenitor (Astrow et al., 1987; Nelson and Weisblat, 1991; Nelson & Weisblat, 1992). Furthermore, teloplasm is enriched with polyadenylated RNA (Astrow et al, 1989; Holton et al., 1994), suggesting that mRNA species associated with teloplasm may act as the molecular determinant of teloblast identities.

However, the molecular identity of the teloblast determinant is currently unknown. Maternal transcript of *Nanos*, as well as its protein product – encoding an RNA binding protein, has been shown to be relatively enriched in the DNOPQ cell (Pilon and Weisblat, 1997; Kang et al., 2002). However, knockdown of Nanos does not affect normal fate specification of these two lineages, despite resulting in morphogenesis defects (Agee et al., 2006). Nonetheless, it is possible that other mRNA than *Nanos*

doi:10.6342/NTU202502160

specifies teloblast identities. Therefore, I aimed to test the hypothesis that a specific set of maternal RNA molecules segregates into the N teloblasts in the series of teloblastogenic asymmetric divisions and thereby determines its identity by characterizing the transcripts that are enriched in the N teloblasts by RNA sequencing and DEG analysis.

I first examined the developmental expression pattern of a previously identified N teloblast-specific gene *Hau-EGL13a*, and found its transcript broadly distributed in all teloblasts at the time of their birth. The expression of *Hau-EGL13a* only becomes restricted to selected teloblasts at later stages. Further, knocking down of *Hau-EGL13a* by the RNA-targeting Cas13d endonuclease does not cause detectible developmental defects in the N teloblast lineage. These results suggest that localized distribution of *Hau-EGL13a* in specific teloblast is not achieved by asymmetric segregation in cell division and that *Hau-EGL13a* is not required for establishing either the teloblast identity or the N identity. To search for more candidates for asymmetrically segregated RNA, I next produced the cell type specific transcriptome for the N teloblast and identified the N-enriched transcripts by DEG analysis. In situ hybridization analysis of the transcripts that are most enriched in the N teloblast showed that these transcripts are not specifically localized to the N teloblast. Further, Gene Ontology enrichment analysis suggested that the identified N enriched transcripts are mostly involved in house-keeping roles. Together, these results rejected the hypothesis that teloblast identity is established through asymmetric segregation of mRNA during cleavage.

doi:10.6342/NTU202502160

Materials and Methods

Laboratory Helobdella austinensis (Hau) culturing

The leeches were raised in 1% artificial seawater (ASW). They were fed frozen pork liver 4-5 times per week, with the water being refreshed 2-4 hours after feeding.

Embryo collection

The gravid leeches were collected from the main colonies and placed in a separate container filled with 1% ASW overnight. After the eggs were laid, the cocoons containing eggs were collected and torn open with tweezers. The eggs were then transferred into a clean culture dish using a glass pipette and washed twice with 1% ASW.

Microinjection

Micropipettes were made by pulling the 1.0mm x 0.75mm glass capillaries (FHC, Inc.) using the Flaming Micropipette Puller (Sutter Instrument). 0.5 μL of injection solution was loaded into a micropipette before microinjection. The injection was performed using the microinjection setup (Crotty & Gann, 2009, pp. 251-255) For lineage tracing, the injection solution consisted of 10 mg/ml tetramethyl rhodamine dextran (RDX; Thermo Fisher) and 0.4% Fast Green FCF (Sigma). For gene knockdown, the injection solution consisted of a specific ratio of in vitro transcribed *Cas13d* mRNA and guidance RNA for the gene of interest, in a solution containing 5 mg/ml RDX and 0.2% Fast Green FCF. The injected embryos were cultured in HL medium containing 10 mg/L tetracycline at 25℃.

doi:10.6342/NTU202502160

Living N teloblasts isolation

Stage 6a embryos were placed in a 1% agar-coated dish containing 1% trypsin, 10 mM DTT, and 50 mM NaOH in HCHL medium for 5 minutes to degrade the vitelline membrane. The cells in the embryos, except for the N teloblasts, were then ablated using an insect pin. The remaining N teloblasts were transferred to a new agar-coated dish with HCHL medium and incubated for 5 minutes. The isolated N teloblasts were subsequently transferred to another agar-coated dish with HL medium and incubated at 25℃.

Time-lapse video recording

Frames of isolated N teloblasts were captured every 5 minutes, with the illumination turned on only during frame capture. These frames were then stacked in chronological order and exported as a 24 fps time-lapse video.

Isolation of N teloblasts in RNAlater

Stage 6a embryos were fixed in RNAlater for 2-3 hours at r.t. or at 4℃ overnight. Then the fixed embryos were transferred to a small droplet of RNAlater on a Sylgard-coated dish. The fixed embryos were broken into single cells by gently squeezing with a glass pin or an insect pin, then the isolated N teloblasts were transferred to a new 1.5 mL microfuge tube containing RNAlater.

RNA extraction

The embryos or cells in RNAlater (Thermo Fisher) were centrifuged at 3500 x g for 20 seconds. Following centrifugation, as much RNAlater as possible was carefully

doi:10.6342/NTU202502160

removed. Subsequently, 200 μL of Tri-reagent (Thermo Fisher) was added to each tube.

The embryos or cells in Tri-reagent were ground using disposable pestles. Following this, 40 μL of 1-Bromo-3-Chloropropane (BCP; Sigma) was added to the Tri-reagent, and the mixture was thoroughly mixed and incubated at r.t. for 10 minutes. The mixture was then centrifuged for 15 minutes at 12000 x g at 4℃ for phase separation. RNA in the aqueous phase was collected and ethanol precipitated.

RNA sequencing

The RNA sequencing was conducted with 3 sets of stage 6a, each 150 embryos, and 3 sets of isolated N teloblasts, each 800 cells, by NovaSeq X Plus 10B 150PE platform with 30G output.

De novo assembly

The sequencing data were analyzed using Trinity 2.13.2 for de novo assembly. Expression levels were calculated with RSEM 1.3.3, and the assembled contigs were subsequently clustered using CD-HIT 4.8.1 to reduce the redundancy. This process was performed on a Linux operating system running Ubuntu 22.04 with kernel version 5.15.0-130-generic.

Differentially expressed genes (DEG) analysis

The DEG analysis was performed using R-4.4.3. The p-value calculation was conducted using a non-paired two-sided Student's t-test. The fold change was calculated using the equation:

$$Fold = log_2(\frac{N_1 + N_2 + N_3}{WE_1 + WE_2 + WE_3})$$

doi:10.6342/NTU202502160

where N_1, N_2, and N_3 represent the gene expression levels of the three replicates of isolated N teloblasts, and WE_1, WE_2, and WE_3 represent the gene expression levels of the three replicates of whole embryos. Sequences with a mean of zero across the expressions of three replicates were discarded.

Gene ontology analysis

The differentially expressed genes were annotated by the transcriptome of *Helobdella robusta* for the ontology analysis. The up-regulated genes were selected based on a fold change greater than 1.5 and a p-value less than 0.05, and were then analyzed by the Panther GO online tool. The GO analysis data was filtered by removing terms with an FDR greater than 0.05.

Preparation of cDNA

The RNA templates were extracted by RNA precipitation from Tri-reagent fixed embryos. And a 20 μL reverse transcription reaction was carried out using RevertAid First Strand cDNA Synthesis Kit (Thermo Fisher). The final cDNA was diluted to a concentration equivalent to the yield from 10ng/μL of RNA.

Probe synthesis

The primers for the specific sequences were designed as in Table 1. The specific sequences were gained by conducting a PCR with the cDNA of stage 6a and the primers, and were then ligated into a TA-cloning vector (pGEM®-T; Promega). The plasmids containing the specific sequences were transformed into competent cells (ECOS™ 101 Competent Cells [DH5α]; Yeastern) by incubation on ice followed by a brief heat-shock

doi:10.6342/NTU202502160

treatment at 42℃ water bath for 40 seconds. The competent cells were spread on a 1.5% agar plate with 2.5% LB broth, 100μg/mL ampicillin. Each plate was supplemented with 40 μL of 0.1M IPTG and 40 μL of 20 mg/mL X-Gal.

Table 1. Primers pairs for probe synthesis.

Sequence ID	Forward primer	Reverse primer
HelroG88096	TTACAGTCAGCACGATGCC	TCGAAACCAGCCAAATCACAT
HelroG168257	TCACCGCCATCTGATACCTT	AGTTCAGACGTGTGCTCTTCC
HelroG191878	ATCGCCGGTGTGACGAAC	GCCCCAATCGCTGTCAGTTA
HelroG174162	GTCACCCTCGAGTCTTGTGA	CCACGATTACGGCGAGGTG
HelroG177726	CCTTGATCTCGATTTCGTTGTTTG	AGGTGAAGAAAGAGATGGCGAA

The plates were incubated at 37℃ overnight, the white colonies were collected and incubated in 5 mL of 2.5% LB broth liquid medium with 100μg/mL ampicillin at 37℃ overnight. 1-2 mL of the liquid medium was taken for plasmid extraction, and the specific sequences on the plasmids were purified after PCR with the M13 primer pair.

The PCR products were then used as templates for *in vitro* transcription using T7 or SP6 RNA polymerase and DIG-labeled NTP. The *in vitro* transcription product was precipitated by adding 1 μL of 0.5M EDTA pH 8 and 4 μL of 6M lithium chloride, followed by the addition of 100 μL of cold 100% EtOH, then stored at 4℃ for 15 minutes.

The PCR products were then used as templates for *in vitro* transcription using T7 or SP6 RNA polymerase and DIG-labeled NTP. The *in vitro* transcription product was precipitated by adding 1 μL of 0.5M EDTA pH 8 and 4 μL of 6M lithium chloride, followed by the addition of 100 μL of cold 100% EtOH, then stored at 4℃ for 15

doi:10.6342/NTU202502160

minutes.

The solution was centrifuged at 16000 x g at 4℃ for 15 minutes, followed by a wash with 75% EtOH and centrifugation at 16000 x g at 4℃ for 5 minutes. The pallets were air-dried for 15 minutes at r.t., and were then resuspended in PreHyb, brought to a final concentration of 100 ng/μL.

In situ hybridization

Samples fixation

Embryos were fixed with 4% PFA in 0.5x PBS (16% PFA:PBS:ddH2O = 1:2:1) at room temperature for 1.5 hours or overnight at 4°C. They were rinsed three times with 1x PBS and then washed three times with 1x PBS for 1 minute each. The embryos were transferred into a silico-coated dish filled with 1x PBS, and the vitelline membrane was removed using the broken pipette method. The embryos were then transferred to a 1.5 mL Eppendorf tube, washed once with 50% MeOH in PBS, and three times with 100% MeOH for 1 minute each. The embryos were stored in 100% MeOH at -20°C for at least three days.

Samples preparation

The embryos fixed in MeOH were washed with 50% MeOH in PBS once, followed by three washes with 0.1% PBTw for 1 minute each. They were then washed with 50% PreHyb in PBTw for 1 minute, followed by two washes with PreHyb for 1 minute each. The embryos were transferred to a new 1.5 mL Eppendorf tube, with less than 50 embryos per tube, and incubated in 200 μL of PreHyb at 68°C overnight.

Hybridization

For hybridization, the PreHyb was replaced with pre-warmed riboprobe (1-10 ng/μL) in PreHyb, and the embryos were incubated at 68°C for 10-48 hours. The

doi:10.6342/NTU202502160

removed PreHyb was collected in another Eppendorf tube and set aside at 68°C.

Probe removal

Probe removal involved washing the embryos with the collected PreHyb at 68°C for 10 minutes, followed by warm washes with 2x SSC once, 0.2x SSC twice, and 0.1x SSC twice, for 20 minutes each. The embryos were allowed to cool to room temperature, rinsed twice with 0.1% PBTw, and washed for 5 minutes in PBTw.

Antibody labeling

For antibody labeling, the embryos were transferred to a 0.6 mL Eppendorf tube using a flamed glass pipette, and all liquid was removed. The embryos were incubated in 500 μL of ab blocking solution at room temperature for 2 hours. After blocking, 0.2 μL of AP-conjugated anti-dig antibody (diluted 1:1 with glycerol) was added to the blocking solution, and the embryos were rocked at 4°C overnight.

Antibody washing

To wash the antibody out, the blocking solution was removed, and the embryos were washed three times with 0.1% PBTw for 1 minute each, followed by six washes with 0.1% PBTw for 20 minutes each.

Color reaction

For the color reaction, the embryos were transferred to a new 1.5 mL microfuge tube, and as much liquid as possible was removed. Then, 100 μL of BM Purple was added, and the embryos were incubated at 37°C until color appeared.

Samples storage

After color reaction, the embryos were rinsed three times with 1x PBS and washed sequentially with 50%, 75%, 87.5%, 93.3%, 100%, and 100% EtOH. The embryos were then stored in EtOH at -20°C.

doi:10.6342/NTU202502160

Cas13d mRNA preparation

0.1 μL of 200x diluted plasmid containing SP6 promoter, coding region of *Cas13d*, SV40 polyadenylation signal sequence, and T3 promoter in sequence was used for the PCR reaction, together with 1 μL of 10 μM SP6 and T3 primers. The PCR product was purified and then used for in vitro transcription with SP6 RNA polymerase at 37℃ overnight. 1 μL of Turbo DNase was added to the *in vitro* transcription reaction and incubated at 37℃ for 15 minutes, followed by a poly A tailing reaction. The synthesized RNA product was purified and made into 0.5 μL aliquots with a concentration of 1μg/μL.

Guiding RNA (gRNA) preparation

The guiding sequences were designed by TIGER online tool (Wessels et al., 2024), and the full-length gRNA was generated through a PCR with a T7 promoter forward primer and a specific guiding sequence reverse primer (Table 2.), followed by a transcription using T7 RNA polymerase.

Table 2. Primers for cas13d guide RNA synthesis.

ID	Sequence
T7 promoter forward	TAATACGACTCACTATAGGAACCCCTACCAACTGGTCGGGGTTTG
GFP reverse	ACATGGTCCTGCTGGAGTTCGTGGTTTCAAACCCCGACCAGTT
HauEGL-13a reverse	GAATCAATTCGTGTTTGGCGCTAGTTTCAAACCCCGACCAGTT

doi:10.6342/NTU202502160

Gene knockdown

The gene knockdown was performed by injecting a mixture of 5 mg/ml RDX, 0.2% fast green, 250 ng of cas13d mRNA, and 100 ng of gRNA in 0.5 μL ddH2O into the D macromere at stage 4a or N teloblast at stage 6a.

doi:10.6342/NTU202502160

Results

Monitoring teloblast development with lineage tracer

Rhodamine dextran (RDX) is an effective intracellular lineage tracer applied by microinjection. Since early cell divisions occur without growth, injected fluorescent dye would remain undiluted, ensuring precise tracking of lineage progression (Duncan et al., 1990). To improve the cellular resolution of lineage-tracing experiments, a tracer consisting of a fusion protein of leech histone 2B and green fluorescent protein (H2B:GFP) was developed (Gline et al., 2009).

I injected RDX together with in vitro transcribed H2B:GFP mRNA into the D' macromere at stage 4a and N at stage 6a (Figure 3, 4). The injection into the D' macromere labeled all teloblasts and their descendant cells with fluorescent signals. While labeling of the N teloblasts marked the ventral nerve cord, including its segmentation and neuron development. Upon observing the D' macromere immediately after injection (0 hours post-injection, hpi), fluorescence was distributed asymmetrically, with a stronger signal in the teloplasm compared to the rest of the cytoplasm (Figure 3a, 3e). A similar pattern was observed in teloblasts M and N, as well as in pre-teloblasts OPQ at 15 hpi (Figure 3b, 3f). By 40 hpi, a substantial number of blast cells had been generated, forming five bandlets on each side (Figure 3c, 3g, 3i). The anterior ends of all bandlets adhered together, while their posterior ends remained attached to the teloblasts. At 65 hpi, all bandlets had aligned to form a pair of germinal bands (Figure 3d, 3h, 3j), which were gradually migrating to the ventral side of the embryo to complete the epiboly process.

In the embryo where N teloblasts had been labeled, the extension and migration of N bandlets were also observed (Figure 4a-c, 4e-g). By 65 hpi, the anterior ends of the

doi:10.6342/NTU202502160

bandlets had fused and differentiated into segmental structures (Figure 4d, 4h, 4i). By the nuclei labeling, the secondary blast cells formation could be clearly observed at 40 hpi (Figure 5). The nuclei of primary blast cells were elliptical, uniformly sized, and neatly arranged (Figure 5a). After division, larger nf.a and smaller nf.p cells, or two equally sized ns.a and ns.p cells, were observed (Figure 5b). Regardless of type, the nuclei of secondary blast cells were rounder compared to those of primary blast cells. Due to the differing division axes of nf and ns, the nuclei of secondary blast cells did not align in a straight line. In the bandlet, two smaller but brighter fluorescence signals were observed within a cell, indicating that a primary blast cell was undergoing division.

Notably, over-injection caused abnormal primary blast cell development. The over-injected n lineage could be distinguished by stronger fluorescence signals of RDX and GFP comparing to normal-injected lineage under identical exposure time (Figure 6). While the over-injected teloblast division remained unaffected initially, the cell cycle halted in primary blast cells, leading to a bandlet deficiency (Figure 6b, 6c). Halted primary blast cells exhibited larger volumes and nuclei compared to normal blast cells, with older cells showing extremely strong nuclei fluorescence, suggesting apoptosis.

***Hau-EGL13a*, a teloblast-localized mRNA, is not required for teloblast identity**

Hau-EGL13a, a member of a protostome-specific *Sox* transcription factor gene subfamily, was previously found as a teloblast-localized transcript in an unpublished in situ hybridization screening of developmental regulatory genes among the embryonic expressed sequence tags (ESTs) generated for the purpose of annotating Helobdella robusta (Simakov et al., 2013). To determine whether *Hau-EGL13a* is necessary for the teloblast identity, I first re-examined its expression pattern by in situ hybridization and

doi:10.6342/NTU202502160

performed knockdown experiments using the RNA-targeting CRISPR-Cas13d technology (Kushawah et al., 2020).

At stage 5, *Hau-EGL13a* exhibits the typical expression pattern of a teloplasm-associated transcript; as its expression is detected in the teloplasm partitions in the M teloblasts and the NOPQ proteloblasts (Figure 7a, 7b). During stage 6, the NOPQ proteloblasts undergo further divisions to generate the four ectoteloblasts. By stage 7, all ectoteloblasts have been formed, and *Hau-EGL13a* expression is restricted to the M and N teloblasts (Figure 7c, 7d). At stage 8, *Hau-EGL13a* signal intensifies in the N teloblasts while disappearing from the M teloblasts (Figure 7e-h). However, at the birth of N teloblasts, *Hau-EGL13a* is not specifically expressed in the N teloblasts, suggesting it is unlikely to play a direct role in N fate specification.

To monitor the efficacy of the Cas13d-mediated knockdown of *Hau-EGL13a* in the leech embryo, Cas13d mRNA and guiding RNA were microinjected into the D' macromere – the precursor cell of all teloblasts, followed by qPCR analysis of RNA extracted from the injected embryos after three days. The results showed a significant reduction in the *Hau-EGL13a* mRNA levels in the knockdown embryos (Figure 8a). To assess phenotypic outcomes, the *Cas13d* mRNA and lineage tracer were co-injected with control (Figure 8b) or either *Hau-EGL13a*-targeting guide RNA (Figure 8c) into the N teloblast. However, no apparent phenotype was observed. In contrast, the GFP fluorescence exhibited significant downregulation in the cells inheriting the control guide RNA targeting GFP. These results suggest that *Hau-EGL13a* may not be involved in the specification of teloblast identity as well as the N identity. However, I cannot rule out the possibility that the absence of a phenotypic change might result from incomplete knockdown. Because of the limited yield of RNA from an individual embryo, it was difficult to evaluate knockdown efficiency at the single-embryo level. Additionally,

doi:10.6342/NTU202502160

based on the results of GFP knockdown, the Cas13d-mediated knockdown does not completely eliminate mRNA, raising the possibility that the small amount of remaining *Hau-EGL13a* transcript was sufficient to maintain its normal function.

Development of blastomere isolation protocol

To identify additional candidate genes involved in N fate specification, I went on to perform a differentially expressed genes (DEG) analysis to uncover N-specific genes. I planned to identify genes that are specifically expressed in N teloblasts using RNA sequencing. To achieve this, I need to isolate N teloblasts from the embryo. I have tested three different approaches: treatment with ACME solution, DTT/trypsin solution, and RNAlater fixation solution.

ACME is a solution that can break the junction between cells. It was designed to dissociate somatic cells of flatworms for single-cell RNA sequencing (Garcia-Castro et al., 2021). Treating tissues with ACME loosens the cell junctions and finally dissociates them into single cells. The ACME protocol was tested in the embryo of the leech *H. austinensis* by adjusting concentration and reaction time. In this experiment, I evaluated ACME at concentrations of 0.5x, 1x, and 2x relative to the flatworm protocol, with reaction times ranging from 2.5 minutes to 20 minutes (Figure 9). Treating the embryos with 0.5x ACME solution slightly loosened the cellular junctions and vitelline membrane in the first 5 minutes, but the cells was not dissociated to single cells completely. The 1x ACME solution degraded both the cellular junctions and the vitelline membrane within 2.5 minutes, demonstrating that leech embryos can be dissociated into single cells using the same method as flatworms. The 2x ACME solution successfully dissociated the cells after 10 minutes; however, the vitelline membrane remained intact until 20 minutes. Prior to its degradation, all cells were

doi:10.6342/NTU202502160

enclosed in an envelope formed by the vitelline membrane.

In all conditions, the teloblasts were separated from the embryo first, followed by the macromeres, while the germinal bands were the last to be dissociated. In most cases, the bandlets retained their band-like structure even after completing the dissociation process. For our purposes, teloblasts could be obtained by adjusting the reaction time and ACME concentration. Moreover, ACME treatment does not affect the fluorescence emission, allowing us to label the N teloblast through microinjection for the identification of dissociated teloblasts and blast cells (Figure 10).

However, following ACME treatment, the dissociated teloblasts remained suspended in solution, making RNA extraction challenging. In the flatworm protocol, suspended cells can be collected via low-speed centrifugation. However, larger cells, such as teloblasts and other embryonic cells, fail to sediment under these conditions. Conversely, high-speed centrifugation led to teloblast rupture. Taken together, these findings indicate that ACME is unsuitable for collecting large blastomeres dissociated from early-stage leech embryos.

Another approach to disrupting intercellular junctions involves using trypsin to degrade membrane proteins that form the cell junctions, thereby separating the cells. This method is commonly used for single-cell sequencing in cultured cells. By treating with trypsin as a preprocessing step, cells can be effectively detached from the medium. For the leech *Helobdella*, the trypsin solution is also used together with DTT for vitelline membrane removal. During this process, the culture medium is adjusted to pH 8.2 by adding NaOH, which is the optimal condition for trypsin activity. DTT reduces disulfide bonds, enhancing the efficiency of vitelline membrane removal.

In this series of experiments, I attempted two methods to isolate N teloblasts. The first method involved directly using DTT/trypsin solution to degrade the junctions

doi:10.6342/NTU202502160

between embryonic cells. This approach required prolonged incubation of the embryos in DTT/trypsin solution to achieve full dissociation. To distinguish N teloblasts from other types of teloblasts, I labeled them using fluorescent dye via microinjection (Figure 11a, 11b). Upon observing the isolated N teloblasts, I noticed that cells subjected to extended DTT/trypsin exposure ceased cell division (Figure 11c). This might be due to damage to membrane-associated proteins linked to the cytoskeleton, preventing the necessary shape changes for mitosis and leading to abnormal cell division. Although this method successfully dissociated the embryo into single cells, the physiological abnormalities observed in the isolated cells could potentially affect subsequent RNA sequencing and differential gene expression analysis. Therefore, I explored an alternative approach.

In this alternative protocol, I first removed the egg membrane using DTT/trypsin, followed by manual dissection using insect pins or glass needles to isolate the N teloblasts. Treatment with the trypsin/DTT solution resulted in over 40% of embryos being devitellinized within the first minute (Figure 12). Within five minutes, nearly 70% of embryos were devitellinized. However, the process slowed thereafter, with only an additional 20% of embryos successfully devitellinized over the next 10 minutes. Most embryos can be successfully devitellinized by treatment with DTT/trypsin solution for 1 minute, which does not affect the normal division.

The surgically separated N teloblasts remained viable in leech embryo culture medium for over 48 hours. Time-lapse imaging revealed that these cells retained their original division pattern. After isolation, the isolated N teloblasts continued cell division independently. From the time-lapse video, the teloblast was observed to protrude and form a budding extension (Figure 13a-b). The connection between the budding extension and teloblast cell body gradually contracted, leading to the formation of a

doi:10.6342/NTU202502160

bulb-like structure (Figure 13c). Eventually, the bulb-like structure separated from the teloblast cell body, resulting in the emergence of a small daughter cell (Figure 13d-f). The teloblast then retracted the remaining parts of budding extension and returned to its original spherical shape (Figure 13g-j). Each division of isolated N teloblasts started at the side proximal to the teloplasm and nucleus, generating a series of anterior-posterior linked progeny cells (Figure 14). This behavior closely resembles how teloblasts in leech embryos generate blast cells, which then arrange into bandlets.

Beyond the similarity in division pattern, the isolated N teloblasts also maintain a stable cell cycle. By measuring the duration of each division, I observed that the first three cell cycles post-surgery generally took longer than usual, but subsequently, the cycle duration stabilized (Figure 15a). After several rounds of stable division, some N teloblasts exhibited progressively longer cell cycles before their division ceased. The number of divisions each isolated N teloblast could undergo varied, yet within different cells, the stable cycles had comparable cycle lengths. From these observations, I infer the fluctuations in cell cycle duration may reflect the physiological state of a cell. Healthy N teloblasts exhibit relatively stable cycle lengths, meaning minimal variation in cycle duration, whereas greater variability suggests that the cell might be experiencing physiological stress.

Since these cells were exposed to DTT/trypsin treatment and isolation surgery, the initially prolonged cell cycles may indicate cells were stressed by the surgical treatment. The subsequent stabilization suggests recovery from this stress. However, for the final few cell cycles, the increasing duration may be attributed to deteriorating culture conditions during time-lapse imaging, which likely exerted physiological stress on the cells, leading to abnormal cycle progression and cessation of division.

In addition to comparing variations in the cell cycle of isolated teloblasts, I also

doi:10.6342/NTU202502160

examined how isolation affects their cell cycle. Experimental results from isolated cell cycles indicate that both surgical impact and environmental stress contribute to prolonged cell cycles. Therefore, before analyzing differences between isolated N teloblasts and the N teloblasts within embryos, it was necessary to exclude cell cycles that were extended due to external stimuli.

By categorizing the division durations of all isolated N teloblasts into 0.2-hour intervals, I observed a peak at approximately 1.5 hours, with a noticeable drop in cycle frequency over 2.4 hours (Figure 15b). Using the 80th percentile threshold (2.41 hours) to filter out abnormal cell cycles, I obtained a mean cell cycle duration of 1.67 hours with a standard deviation of 0.17. In contrast, non-isolated N teloblasts had a mean cycle duration of 1.63 hours with a standard deviation of 0.04. A Student's t-test yielded a p-value of 0.38, indicating no significant difference between the two conditions (Figure 15c).

In summary, I confirmed that isolated N teloblasts can independently undergo cell division to generate blast cells, and their cell cycle remains consistent with that of N teloblasts during normal embryonic development. This result indicates that N teloblasts possess an autonomous regulatory mechanism that allows them to continuously produce primary blast cells. Even in the absence of any external signals, they are still able to maintain a normal cell cycle for generating primary blast cells.

Compared to directly dissociating embryos by ACME, using a DTT/trypsin solution to remove the egg membrane and then surgically isolating N teloblasts allows for the retrieval of living cells, which is beneficial for subsequent RNA extraction. However, performing surgery on living embryos is time-consuming, and all embryos must undergo the procedure at stage 6a. These constraints significantly limit the number of samples collected per experiment. To address this, I applied a new isolation method

doi:10.6342/NTU202502160

with a fixing solution—RNAlater.

RNAlater is a solution containing high salt concentration that effectively preserves RNA in samples. In addition, it makes cells more “rubber-like”, which improves surgical tolerance. RNAlater also compensates for the limitations of ACME. Its high salt concentration increases cell density, allowing for easy sedimentation through low-speed centrifugation. Furthermore, it enables embryos to be fixed at a specific stage, optimizing their usability. Considering these advantages, I ultimately used RNAlater to fix stage 6a leech embryos and isolated N teloblast cells using insect pins for RNA extraction and sequencing.

Production of the N teloblast transcriptome: RNA sequencing and data processing

I collected three batches of isolated N teloblasts along with three batches of stage 6a whole embryos for RNA sequencing, yielding three biological replicates of N-specific libraries and three replicates of whole-embryo libraries. For de novo assembly and expression level calculation, I used Trinity 2.13.2 and RSEM 1.3.3. The results yielded 63,931 contigs—significantly more than the expected number of coding genes in their sibling species *H. robusta*, which had only 23432 coding genes according to the EnsemblMetazoa. This redundancy is likely due to the presence of duplicated contigs. To address this, CD-HIT was applied for contig clustering. CD-HIT reconstructs the dataset by grouping highly similar sequences into a cluster, and chooses the longest one as the representative sequence for each cluster. Additionally, the dataset was also annotated using the transcriptome derived from the genome annotation of *Helobdella robusta* (Hro), a sibling species of *Helobdella austinensis*. The reconstructed datasets were further analyzed using principal components analysis (PCA).

doi:10.6342/NTU202502160

All PCAs were performed using the expression levels of individual genes as the components. In the PCA of Trinity-RSEM data, WE and N samples formed two distinct clusters, indicating significant differences in gene expression patterns between WE and N. Notably, the data points in cluster N were more dispersed, suggesting higher variability within N compared to WE.

A series of CD-HIT clustering analyses with varying parameters was performed, followed by PCA to assess the results. First, the parameter "similarity" was varied from 0.9 to 0.5 in decrements of 0.1 (Figure 16). As the similarity threshold decreased, the distribution of points in the PCA shifted. Specifically, with decreasing similarity, the points within the WE and N clusters moved closer to their respective centers along the PC1 axis while dispersing outward along the PC2 axis. By a similarity of 0.5, the distinction between WE and N blurred, with the points forming a linear pattern along the PC2 axis.

Across a range of similarity changes, a notable shift was observed between similarity values of 0.5 and 0.6. To examine this transition in more detail, further analysis was conducted at intervals of 0.01 within this range. The results revealed that the WE and N clusters were most distinct at a similarity of 0.54, where the separation along the PC2 axis reached the minimum while the spread along the PC1 axis remained relatively low.

Next, the "coverage" parameter, representing the percentage of aligned length relative to the total sequence length, was adjusted at a similarity of 0.54. Only alignments exceeding the coverage threshold were included in the same cluster. I examined coverage values ranging from 0.5 to 0.9 in increments of 0.1 (Figure 17). Interestingly, these adjustments had no impact on the PCA results, indicating that RNA-seq redundancy was driven by sequence variability rather than low read coverage.

doi:10.6342/NTU202502160

In the PCA of CD-HIT clustered data with a similarity above 0.54 and coverage exceeding 0.9, WE and N samples remained as two distinct clusters. However, the distances within each cluster were reduced, suggesting that CD-HIT clustering successfully minimized deviations among data points without compromising the separation between WE and N groups.

In the PCA of Hro annotated data, WE and N clusters remained clearly distinct. Furthermore, the distances between data points within each cluster were significantly reduced compared to Trinity-RSEM and CD-HIT clustered data, demonstrating an enhanced ability to mitigate bias (Figure 18).

Identification of differentially expressed genes

The CD-HIT clustered dataset closely resembles both the *H. robusta* and *H. austinensis* transcriptomes. It contains 18313 contigs with an average length of 1378 bps, similar to the *H. robusta* transcriptome, which comprises 23432 genes with an average contig length of 1239 bps, as reported by the Joint Genome Institute (JGI). Likewise, the *H. austinensis* transcriptome at stage 0–1 consists of 18954 transcripts (Hsiao, 2024). The Hro annotated dataset contains 11780 genes with an average length of 1632 bps. This dataset more resembles to the transcriptome of *H. austinensis* stage 10 embryo, which has 13753 annotated transcripts (Kwak, 2022).

Although both the CD-HIT clustered dataset and the Hro annotated dataset successfully grouped the six datasets into two clusters—isolated N teloblasts and whole embryos— and resembled the reference transcriptome, CD-HIT required lowering the similarity threshold to 0.54 to achieve results comparable to the Hro annotated dataset. This suggests that the CD-HIT clustered dataset is less reliable. In contrast, the Hro annotated dataset identifies similar sequences using BLAST, considering only those

doi:10.6342/NTU202502160

with an e-value below 10^{-30} as the same gene, making it more trustworthy. Therefore, subsequent DEG analysis was conducted primarily using the Hro annotated dataset.

The Hro annotated dataset identified 11,598 non-zero-expressed genes, with 11,243 detected in whole embryos (WE) and 11,113 detected in isolated N teloblasts (N). Among the total 11,598 genes, 10,758 were present in both WE and N, while 485 were exclusive to WE and 355 were exclusive to N (Figure 19a). However, in the experimental design, genes expressed only in N should not exist, as WE already contained N teloblasts. To further clarify this result, I analyzed the expression distribution of these exclusively expressed genes and found that highly expressed genes generally showed no differential expression between WE and N, with a correlation coefficient of 0.97 (Figure 19b). Additionally, the differentially expressed genes only exhibit low expression level (Figure 19c). DEG analysis revealed that most genes showed no significant expression differences between isolated N teloblasts and whole embryos. Most of the differentially expressed genes had low expression levels, increasing the possibility that the observed differences might stem from sampling variability rather than true differential expression. Notably, in the DEG analysis, the gene HelroG88096, which encodes a ubiquitin-specific protease (USP) domain-containing protein, which is responsible for removing ubiquitin from ubiquitin conjugates (Wilkinson, 2000; Fischer, 2003), had the highest significant fold change (Figure 19d).

A comparative analysis across different datasets identified three N-enriched genes—HelroG168257, HelroG191878, and HelroG174162—which encode CCDC92_74 N-terminal domain-containing protein, CUB domain-containing protein, and Fibronectin type-III domain-containing protein, respectively (Figure 19d). These genes were recognized for exhibiting statistically significant upregulation in both the

doi:10.6342/NTU202502160

CD-HIT clustered dataset and the Hro annotated dataset. I also examined the N-deficient genes and identified a significantly deficient gene, HelroG177726. However, since it is an uncharacterized protein, its role in embryonic development remains unclear.

Validating the DEG analysis with in situ hybridization

I cloned the candidate genes identified from the DEG analysis—including four N-enriched genes HelroG88096, HelroG168257, HelroG191878, HelroG174162, and a N-deficient gene HelroG177726—from stage 6a cDNA and synthesized dig-labeled riboprobes for *in situ* hybridization. Since these candidate genes exhibit low expression levels, the color reaction duration was set to stop when either all embryos displayed a signal or when more than half of them developed background noise.

In the *in situ* hybridization results for the N-enriched genes HelroG88096 and HelroG168257, N teloblasts and OPQ proteloblasts showed faint signals within the teloplasm (Figure 20a, 20b). However, for HelroG191878 and HelroG174162, signals were almost undetectable in teloblasts (Figure 20c, 20d). Overall, all signals were weaker than the background noise and broadly distributed across N teloblasts and OPQ proteloblasts, indicating that these N-enriched genes exhibit low and non-specific expression. In the result of N-deficient gene HelroG177726, M teloblasts exhibit the strongest signal in the teloplasm whereas N teloblasts show no signal (Figure 21).

Gene Ontology enrichments among the differentially expressed genes

In addition to in situ hybridization, I conducted gene ontology (GO) analysis based on the results of the DEG analysis. When applying a two-fold change threshold for N-enriched genes, no enriched GO terms were identified. This outcome could be

doi:10.6342/NTU202502160

attributed to two possible reasons: either there are no distinctly enriched genes in N teloblast, suggesting that N teloblast identification is not regulated by the expression of specific genes, or the fold-change threshold setting is suboptimal.

Since my DEG analysis compares isolated N teloblasts with whole embryos, and N teloblasts are also present within the whole embryo, the gene expression differences may be diluted. To address this, I adjusted the fold-change threshold to 1.5-fold and reran the GO analysis (Figure 22). In the Biological Process category, protein transport had the highest enrichment score, followed by carbohydrate and phosphate metabolism and protein localization-related GO terms. In the Cellular Component category, lysosome and lytic vacuole had the highest enrichment scores, with other enriched GO terms predominantly linked to organelles, particularly membrane-bound organelles. In the Molecular Function category, nucleotide binding had the highest enrichment score. Notably, no GO terms related to development, differentiation, or transcription factors were identified, indicating that the intrinsic regulatory mechanism of N teloblasts is not governed by differential gene expression.

The N-deficient genes were also taken for GO analysis (Figure 23). In the Biological Process category, glutamate metabolic process had the highest enrichment score, followed by zinc ion transmembrane transport and RNA metabolic process-related GO terms, including RNA biosynthesis and splicing. In the Cellular Component category, tRNA-intron endonuclease complex exhibited a very high enrichment score, followed by exocyst, vesicle tethering complex, and ribosome-related GO terms, which are involved in protein biosynthesis. In the Molecular Function category, GO terms associated with enzyme activity had higher enrichment scores.

Through GO analysis, most enriched genes in N teloblasts were linked to general cellular physiology, whereas N-deficient genes were primarily associated with RNA

doi:10.6342/NTU202502160

biosynthesis, modification, and protein biosynthesis. These findings suggest that N teloblast determination is not defined by asymmetric segregation of specific RNA molecules.

doi:10.6342/NTU202502160

Discussion

To investigate the potential role of localized mRNA as the fate determinant in the specification of teloblast fate in the leech embryo, I characterized the expression patterns and the functional requirement of *Hau-EGL13a* in N teloblast fate specification through in situ hybridization and targeted knockdown using Cas13d. Although *Hau-EGL13a* was initially identified as a teloblast-specific gene, its expression dynamics across developmental stages preclude its role as the N fate determinant. Notably, *Hau-EGL13a* was not specifically expressed in N teloblasts at the time of their birth (Figure 7), implicating it as a regulator of later developmental events in teloblasts rather than a determinant of initial cell fate.

Functional analysis via Cas13d-mediated knockdown further supported this notion. Despite a reduction in *Hau-EGL13a* transcript levels confirmed by qPCR, no apparent developmental phenotype was observed following knockdown in N teloblasts (Figure 8). This lack of phenotypic change may indicate that *Hau-EGL13a* is not involved in bandlet formation. These results suggest that EGL-13 may not serve as a primary regulator of N fate specification. However, technical limitations—such as limited efficacy of RNA knockdown and the difficulty in extracting RNA from individual embryos—leave open the possibility that residual *Hau-EGL13a* transcripts may be enough to maintain the normal phenotype.

Next, I established a protocol for teloblast isolation and examined their division behaviors and cell cycle dynamics. Observations revealed that isolated N teloblasts behaved similarly to those in intact embryos, suggesting that teloblast proliferation is governed by an intrinsic mechanism (Figure 13, 14 and 15).

Using this protocol, I performed RNA sequencing and DEG analysis to identify

doi:10.6342/NTU202502160

differentially expressed genes between the isolated N teloblast and the whole embryo. I found that low-expression genes HelroG88096, HelroG168257, HelroG191878, and HelroG174162 were significantly enriched in N teloblasts compared to whole embryos (Figure 19). However, in situ hybridization revealed that these N-enriched genes exhibited only faint signals and were not specifically expressed in N teloblasts (Figure 20). The most enriched GO terms in N teloblasts included lysosome and lytic vacuole, along with phosphate metabolic process and nucleotide binding—suggesting their roles are related to general cellular physiology rather than fate specification (Figure 22).

In the early embryonic development of the mollusk *Ilyanassa obsoleta*, *IoEve*, *IoDpp*, and *IoTld* are identified as determinants that are asymmetrically inherited during cleavage (Lambert & Nagy, 2002). *IoEve*, a homolog of *even-skipped* homeobox transcription factor, is involved in patterning cells along the animal–vegetal axis, while *IoDpp*, the homolog of vertebrate bmp2/4, and *IoTld*, a protease that releases BMP ligands from chordin inhibition, contribute to head precursor cell specification. Similarly, in the arthropod *Drosophila melanogaster*, the maternal mRNAs *bicoid*, *nanos*, and *oskar* are spatially localized during oogenesis and translated in the early embryo (Lasko, 2012), playing essential roles in anterior–posterior axis formation and germ cell specification. All of these genes are well-known for their critical roles in embryonic development. In contrast, the N-enriched genes we identified do not appear to exert similarly pronounced effects on embryogenesis.

Conversely, the N-deficient gene HelroG177726 was specifically detected in M teloblasts via in situ hybridization (Figure 21). While this gene remains uncharacterized, further functional analysis is necessary. GO analysis of the N-deficient genes revealed that enriched terms included glutamate metabolic process, zinc ion transmembrane transport, tRNA-intron endonuclease complex, and exocyst, along with protein

doi:10.6342/NTU202502160

synthesis, localization, and interaction (Figure 23). The GO analysis shows N-deficient genes are more likely involved in protein biosynthesis. Interestingly, some of the N-deficient GO terms, such as RNA splicing, cellular localization, gene expression and GTPase regulator activity, appeared more relevant to teloblast fate determination than the N-enriched ones.

Based on DEG and GO analysis, the hypothesis that asymmetric segregation of RNA fate determinant specifies the N teloblast cell fate was rejected. There are two possible alternative hypotheses for the specification of teloblast identity. First, N fate specification may not be induced by the expression of N-specific genes, but rather by the absence of exclusive determinants necessary for the alternative fate. Second, the determinants may not be RNA-based, as transcriptome profiling only assesses gene expression at the RNA level, while proteins could also play a crucial role. In the N-enriched genes, USP proteins and lysosomes are key components of maternal protein degradation during early embryonic development (Toralova, 2020), whereas N-deficient genes are associated with protein synthesis, suggesting differences in protein-level regulation between N teloblasts and whole embryos.

One of the most well-characterized examples of protein localization-dependent embryonic development involves the PAR proteins. PAR proteins are a conserved family of scaffolding and regulatory molecules essential for establishing cell polarity in animals. In *Caenorhabditis elegans*, they orchestrate anterior–posterior axis formation in the zygote following fertilization. Anterior proteins such as PAR-3, PAR-6, and PKC-3 accumulate at the anterior cortex, while PAR-1 and PAR-2 localize to the posterior— a distribution initiated by a sperm-derived cue and stabilized through mutual antagonism between these two groups (Kemphues et al., 1988; Etemad-Moghadam et al., 1995; Boyd et al., 1996). These mechanisms are not only critical for *C. elegans*

doi:10.6342/NTU202502160

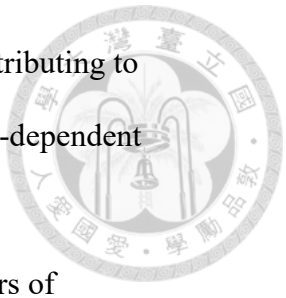

embryogenesis but are also broadly conserved across metazoans, contributing to epithelial polarity, neuroblast asymmetric division, and other polarity-dependent processes.

In *Drosophila melanogaster*, Bicoid and Nanos are key regulators of anterior–posterior axis specification. Bicoid, a homeodomain-containing transcription factor, is localized to the anterior of the oocyte during oogenesis. Its concentration gradient functions as a morphogen, activating anterior-specific genes such as hunchback while repressing the translation of posterior determinants like caudal mRNA (Driever & Nüsslein-Volhard, 1988; Struhl et al., 1989). In contrast, Nanos localizes to the posterior pole and promotes posterior cell fate specification (Lehmann & Nüsslein-Volhard, 1991; Irish et al., 1989).

These diverse examples collectively underscore the critical role of protein localization in embryonic development. Given the enrichment of lysosome-related genes and USP domain-containing genes, future proteomic studies will be essential for uncovering protein-based mechanisms underlying N teloblast determination.

doi:10.6342/NTU202502160

References

Agee, S. J., Lyons, D. C., & Weisblat, D. A. (2006). Maternal expression of a NANOS homolog is required for early development of the leech Helobdella robusta. Developmental Biology, 298(1), 1–11. https://doi.org/10.1016/j.ydbio.2006.06.021

Astrow, S., Holton, B., & Weisblat, D. A. (1987). Centrifugation redistributes factors determining cleavage patterns in leech embryos. Developmental Biology, 120(2), 270–283. https://doi.org/10.1016/0012-1606(87)90164-X

Beloussov, L. V., & Meshcheryakov, V. N. (1975). Asymmetrical rotations of blastomeres in early cleavage of gastropoda. Wilhelm Roux's Archives of Developmental Biology, 177, 193–203. https://doi.org/10.1007/BF00848234

Bissen, S. T., & Weisblat, D. A. (1987). Early differences between alternate n blast cells in leech embryo. Journal of Neurobiology, 18(3), 251–269. https://doi.org/10.1002/neu.480180306

Bissen, S. T., & Weisblat, D. A. (1989). The durations and compositions of cell cycles in embryos of the leech, Helobdella triserialis. Development, 106(1), 105–118. https://doi.org/10.1242/dev.106.1.105

Boyd, L., Guo, S., Levitan, D., Stinchcomb, D. T., & Kemphues, K. J. (1996). PAR-2 is asymmetrically distributed and promotes association of P granules and PAR-1 with the cortex in C. elegans embryos. Development, 122(10), 3075–3084. https://doi.org/10.1242/dev.122.10.3075

Crotty, D. A., & Gann, A. (Eds.). (2009). *Emerging model organisms: A laboratory manual* (Vol. 1). Cold Spring Harbor Laboratory Press.

Driever, W., & Nüsslein-Volhard, C. (1988). A gradient of bicoid protein in Drosophila embryos. Cell, 54(1), 83–93. https://doi.org/10.1016/0092-8674(88)90182-1

doi:10.6342/NTU202502160

Etemad-Moghadam, B., Guo, S., & Kemphues, K. J. (1995). Asymmetrically distributed PAR-3 protein contributes to cell polarity and spindle alignment in early C. elegans embryos. Cell, 83(5), 743–752. https://doi.org/10.1016/0092-8674(95)90188-3

Fernandez, J., & Stent, G. S. (1980). Embryonic development of the glossiphoniid leech Theromyzon rude: Structure and development of the germinal band. Developmental Biology, 78, 407–434. https://doi.org/10.1016/0012-1606(80)90344-9

Fischer, J. A. (2003). Deubiquitinating enzymes: Their roles in development, differentiation, and disease. International Review of Cytology, 229, 43–72. https://doi.org/10.1016/S0074-7696(03)01002-4

Gline, S. E., Kuo, D. H., Stolfi, A., & Weisblat, D. A. (2009). High resolution cell lineage tracing reveals developmental variability in leech. Developmental Dynamics, 238(12), 3139–3151. https://doi.org/10.1002/dvdy.22131

Gline, S. E., Nakamoto, A., Cho, S. J., Chi, C., & Weisblat, D. A. (2011). Lineage analysis of micromere 4d, a super-phylotypic cell for Lophotrochozoa, in the leech Helobdella and the sludgeworm Tubifex. Developmental Biology, 353(1), 120–133. https://doi.org/10.1016/j.ydbio.2011.02.016

Henry, J. J., Perry, K. J., Fukui, L., & Alvi, N. (2010). Differential localization of mRNAs during early development in the mollusc, Crepidula fornicata. Integrative and Comparative Biology, 50(5), 720–733. https://doi.org/10.1093/icb/icq098

Henry, J. Q. (2014). Spiralian model systems. International Journal of Developmental Biology, 58, 389–401. https://doi.org/10.1387/ijdb.140108jh

Holton, B., Wedeen, C. J., Astrow, S. H., & Weisblat, D. A. (1994). Localization of polyadenylated RNAs during teloplasm formation and cleavage in leech embryos.

doi:10.6342/NTU202502160

Roux's Archives of Developmental Biology, 204(1), 46–53. https://doi.org/10.1007/BF01419471

Hsaio, S., Saglam, N., Morrow, D., & Shain, D. H. (2024). Transcriptomic profiling at the maternal-to-zygotic transition in leech, Helobdella austinensis. Genes, 15(3), 283. https://doi.org/10.3390/genes15030283

Huang, F. Z., Kang, D., Ramirez-Weber, F. A., Bissen, S. T., & Weisblat, D. A. (2002). Micromere lineage in the glossiphoniid leech Helobdella. Development, 129(3), 719–732. https://doi.org/10.1242/dev.129.3.719

Irish, V., Lehmann, R., & Akam, M. (1989). The Drosophila posterior-group gene nanos functions by repressing hunchback activity. Nature, 338(6217), 646–648. https://doi.org/10.1038/338646a0

Kang, D., Pilon, M., & Weisblat, D. A. (2002). Maternal and zygotic expression of a nanos-class gene in the leech Helobdella robusta: Primordial germ cells arise from segmental mesoderm. Developmental Biology, 245(1), 28–41. https://doi.org/10.1006/dbio.2002.0610

Kemphues, K. J., Priess, J. R., Morton, D. G., & Cheng, N. S. (1988). Identification of genes required for cytoplasmic localization in early C. elegans embryos. Cell, 52(3), 311–320. https://doi.org/10.1016/0092-8674(88)90526-5

Knoblich, J. A. (2008). Mechanisms of asymmetric stem cell division. Cell, 132(4), 583–597. https://doi.org/10.1016/j.cell.2008.02.007

Kuo, D.-H. (2017). The polychaete-to-clitellate transition: An EvoDevo perspective. Developmental Biology, 427(2), 230–240. https://doi.org/10.1016/j.ydbio.2017.04.002

Kuo, D. H., & Hsiao, Y. H. (2018). Duplicated FoxA genes in the leech Helobdella: Insights into the evolution of direct development in clitellate annelids.

doi:10.6342/NTU202502160

Developmental Dynamics, 247(5), 763-778.

Kwak, H. J., Lee, S. G., Park, S. C., Kim, J. H., Weisblat, D. A., Park, C., & Cho, S. J. (2022). Head transcriptome profiling of glossiphoniid leech (Helobdella austinensis) reveals clues about proboscis development. Open Biology, 12(3), 210298. https://doi.org/10.1098/rsob.210298

Lambert, J. D., & Nagy, L. M. (2002). Asymmetric inheritance of centrosomally localized mRNAs during embryonic cleavages. Nature, 420(6916), 682–686. https://doi.org/10.1038/nature01264

Lasko, P. (2012). mRNA localization and translational control in Drosophila oogenesis. Cold Spring Harbor Perspectives in Biology, 4(10), a012294. https://doi.org/10.1101/cshperspect.a012294

Lehmann, R., & Nüsslein-Volhard, C. (1991). The maternal gene nanos has a central role in posterior pattern formation of the Drosophila embryo. Development, 112(3), 679–691. https://doi.org/10.1242/dev.112.3.679

Martín-Durán, J. M., & Marlétaz, F. (2020). Unravelling spiral cleavage. Development, 147(1), dev181081. https://doi.org/10.1242/dev.181081

Martindale, M., & Shankland, M. (1990). Intrinsic segmental identity of segmental founder cells of the leech embryo. Nature, 347, 672–674. https://doi.org/10.1038/347672a0

Nakamoto, A., Nagy, L. M., & Shimizu, T. (2011). Secondary embryonic axis formation by transplantation of D quadrant micromeres in an oligochaete annelid. Development, 138(2), 283–290. https://doi.org/10.1242/dev.057703

Nelson, B. H., & Weisblat, D. A. (1991). Conversion of ectoderm to mesoderm by cytoplasmic extrusion in leech embryos. Science, 253(5021), 435–438. https://doi.org/10.1126/science.1857960

doi:10.6342/NTU202502160

Nishida, H., & Sawada, K. (2001). macho-1 encodes a localized mRNA in ascidian eggs that specifies muscle fate during embryogenesis. Nature, 409(6821), 724–729. https://doi.org/10.1038/35055568

Pilon, M., & Weisblat, D. A. (1997). A nanos homolog in leech. Development, 124(9), 1771–1780. https://doi.org/10.1242/dev.124.9.1771

Ramirez, F. A. (1995). Morphogenesis and engrailed-class gene expression during development of the glossiphoniid leech central nervous system [Doctoral dissertation, University of California, Berkeley].

Seudre, O., Carrillo-Baltodano, A. M., Liang, Y., & Martín-Durán, J. M. (2022). ERK1/2 is an ancestral organising signal in spiral cleavage. Nature Communications, 13, 2286. https://doi.org/10.1038/s41467-022-29970-6

Shain, D. H., Stuart, D. K., Huang, F. Z., & Weisblat, D. A. (2000). Segmentation of the central nervous system in leech. Development, 127(4), 735–744. https://doi.org/10.1242/dev.127.4.735

Shlyakhtina, Y., Moran, K. L., & Portal, M. M. (2019). Asymmetric inheritance of cell fate determinants: Focus on RNA. Non-coding RNA, 5(2), 38. https://doi.org/10.3390/ncrna5020038

Simakov, O., Marlétaz, F., Cho, S. J., Edsinger-Gonzales, E., Havlak, P., Hellsten, U., … Rokshar, D. S. (2013). Insights into bilaterian evolution from three spiralian genomes. Nature, 493(7433), 526–531. https://doi.org/10.1038/nature11696

Smith, C. M., Lans, D., & Weisblat, D. A. (1996). Cellular mechanisms of epiboly in leech embryos. Development, 122(6), 1885–1894. https://doi.org/10.1242/dev.122.6.1885

Toralova, T., Kinterova, V., Chmelikova, E., & Kanka, J. (2020). The neglected part of early embryonic development: Maternal protein degradation. Cellular and

doi:10.6342/NTU202502160

Molecular Life Sciences, 77, 3177–3194. https://doi.org/10.1007/s00018-020-03488-2

Weisblat, D. A., & Huang, F. Z. (2001). An overview of glossiphoniid leech development. Canadian Journal of Zoology, 79(2), 218–232. https://doi.org/10.1139/z00-195

Weisblat, D. A., & Kuo, D. H. (2014). Developmental biology of the leech Helobdella. International Journal of Developmental Biology, 58, 429–438. https://doi.org/10.1387/ijdb.140105dw

Weisblat, D. A., Sawyer, R. T., & Stent, G. S. (1978). Cell lineage analysis by intracellular injection of a tracer enzyme. Science, 202(4371), 1295–1298. https://doi.org/10.1126/science.725605

Weisblat, D. A., & Shankland, M. (1985). Cell lineage and segmentation in the leech. Philosophical Transactions of the Royal Society of London. Series B, Biological Sciences, 312(1153), 39–56. https://doi.org/10.1098/rstb.1985.0003

Wessels, H.-H., Stirn, A., Méndez-Mancilla, A., Kim, E. J., Hart, S. K., Knowles, D. A., & Sanjana, N. E. (2024). Prediction of on-target and off-target activity of CRISPR-Cas13d guide RNAs using deep learning. Nature Biotechnology, 42, 628–637. https://doi.org/10.1038/s41587-023-01991-y

Whitman, C. O. (1878). The embryology of Clepsine. Quarterly Journal of Microscopical Science, 18, 213–315.

Whitman, C. O. (1887). A contribution to the history of the germ-layer in Clepsine. Journal of Morphology, 1, 105–182.

Wilkinson, K. D. (2000). Ubiquitination and deubiquitination: Targeting of proteins for degradation by the proteasome. Seminars in Cell & Developmental Biology, 11(3), 141–148. https://doi.org/10.1006/scdb.2000.0167

doi:10.6342/NTU202502160

Zackson, S. L. (1982). Cell clones and segmentation in leech development. Cell, 31(3 Pt 2), 761–770. https://doi.org/10.1016/0092-8674(82)90337-2

Zackson, S. L. (1984). Cell lineage, cell-cell interaction, and segment formation in the ectoderm of a glossiphoniid leech embryo. Developmental Biology, 104(1), 143–160. https://doi.org/10.1016/0012-1606(84)90017-7

Zhang, S. O., Kuo, D. H., & Weisblat, D. A. (2009). Grandparental stem cells in leech segmentation: Differences in CDC42 expression are correlated with an alternating pattern of blast cell fates. Developmental Biology, 336(1), 112–121. https://doi.org/10.1016/j.ydbio.2009.09.015

doi:10.6342/NTU202502160

Figures

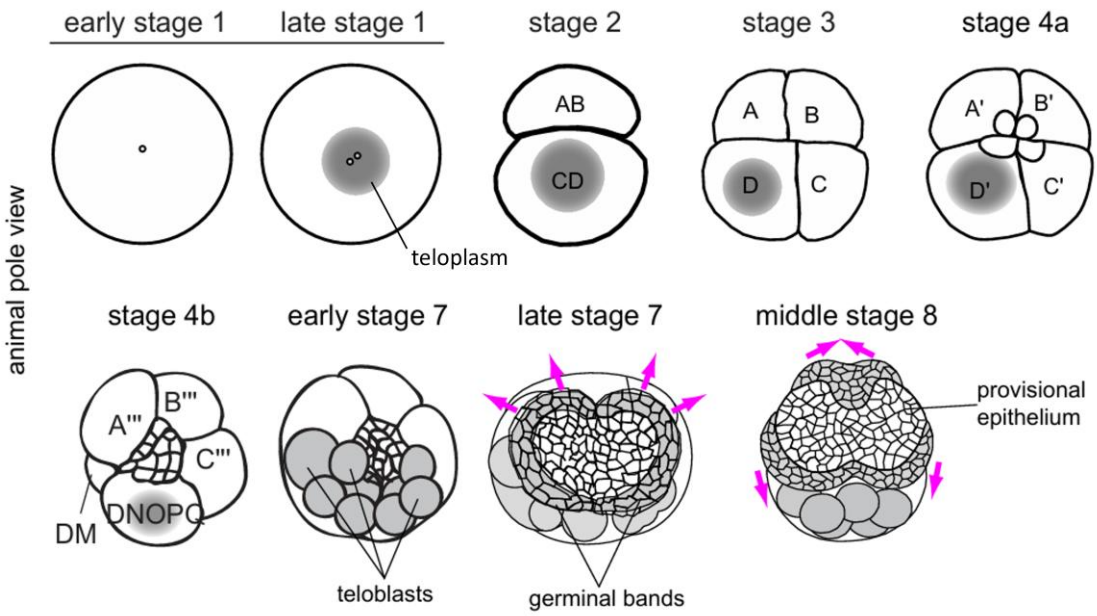

Figure 1. Developmental process of a leech embryo. The embryo undergoes spiral cleavage, giving rise to four quadrants. RNA-enriched teloplasm concentrates in the D quadrant and subsequently segregates into five pairs of teloblasts. Teloblasts exhibit iterated asymmetric divisions, generating a series of homologous blast cells—also known as segmental founder cells. These blast cells form two band-like structures called germinal bands, which migrate toward the vegetal pole during gastrulation. Eventually, the two germinal bands fuse at the ventral midline, developing into the leech body. This figure is adapted from Kuo and Hsiao (2018).

doi:10.6342/NTU202502160

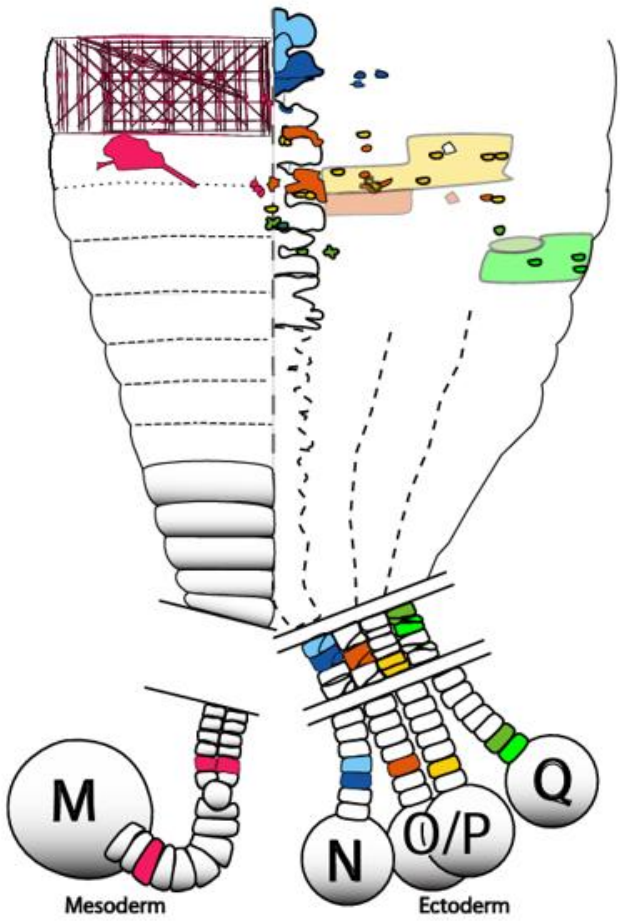

Figure 2. Developmental pattern of teloblast lineages. The M lineage develops into mesodermal tissue, whereas the N, O, P, and Q lineages differentiate into ectodermal tissue. The N lineage primarily contributes to the ventral nerve cord, which constitutes the central nervous system (CNS) in the leech. The Q lineage gives rise to peripheral neurons. The O and P lineages contribute to portions of the CNS and peripheral neurons. This figure is adapted from Weisblat and Kuo (2014).

doi:10.6342/NTU202502160

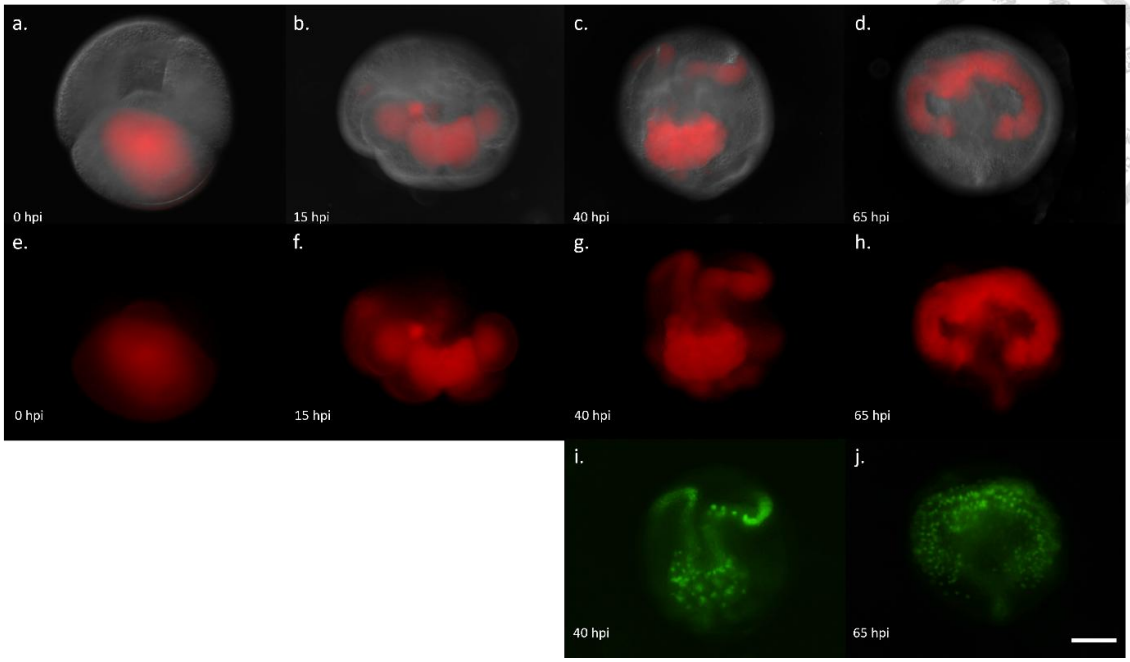

Figure 3. RDX and H2B:GFP mRNA injection in D' macromere. The D' macromere was injected at 8 hour-post-fertilization (hpf) along with RDX and H2B:GFP mRNA, RDX labeled the cytoplasm while H2B:GFP labeled the nuclei. (a-d) are composites combining dark field and red fluorescence channels, (e-h) are red fluorescence only, (i-j) are green fluorescence only. After injection (0 hour-post-injection, 0 hpi), the macromere D' was labeled by red fluorescent (a, e). All images were taken from animal pole. Teloplasm exhibited a stronger signal compared to the surrounding region of cytoplasm. The fluorescent dye was dispersed into teloblasts M, N and OPQ at 15 hpi (b, f). At 40 hpi, numerous blast cells had formed, with their anterior ends adhering to one another while their posterior ends remained attached to the teloblasts (c, g, i). At 65 hpi, all bandlets aligned and lengthened, as epiboly progressed (d, h, j). Scale bar: 100 μm.

doi:10.6342/NTU202502160

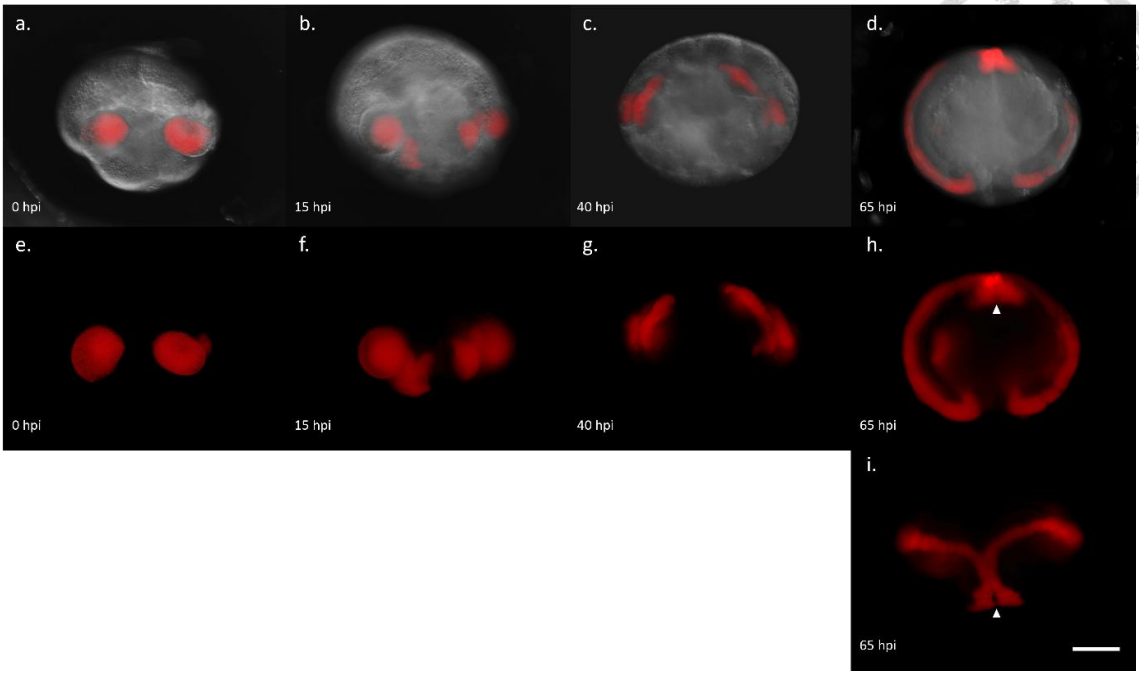

Figure 4. RDX and H2B:GFP mRNA injection in N teloblasts. The N teloblasts were injected at 20 hpf along with RDX and H2B:GFP mRNA, RDX labeled the cytoplasm while H2B:GFP labeled the nuclei. (a-d) are composites combining dark field and red fluorescence channels, (e-i) are red fluorescence only. (a-h) are taken from animal pole, while (i) was taken from ventral side. N teloblasts divided rapidly, generating two bandlets bilaterally (a-c, e-f). At 65 hpi, the anterior most parts of N bandlets fused and differentiated to segmental structure (d, h, i). The white arrowheads in (h) and (i) indicate the identical structure from different perspectives. Scale bar: 100 μm.

doi:10.6342/NTU202502160

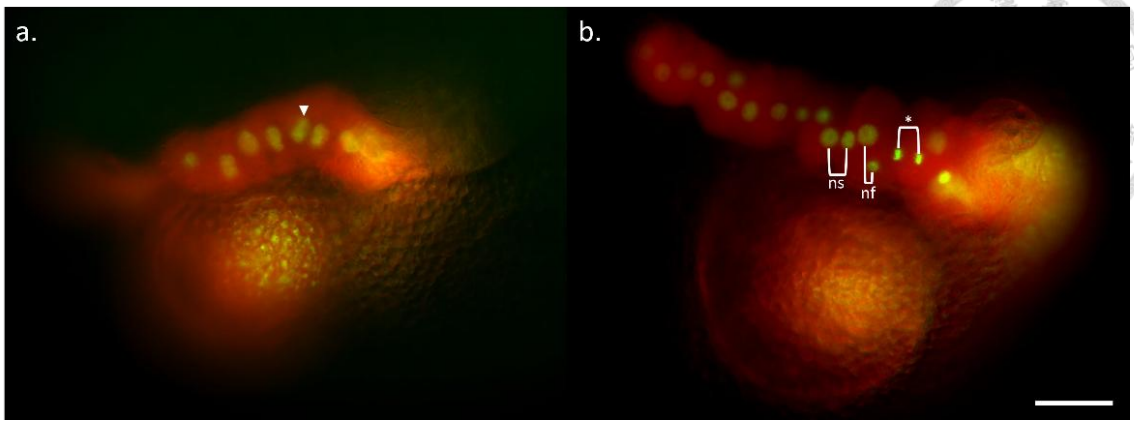

Figure 5. Blast cells in N lineage at 50 hpi. The nuclei of primary blast cells (white arrowhead in a) were elliptical and arranged neatly compared to secondary blast cell (b). The secondary blast cells can be distinguished by their nuclei size and arrangement. Descendents of ns, ns.a and ns.p, were identical in nuclei size (marked as ns in b). However, nf divided into two cells with unequal sized nuclei, a smaller nf.a and a larger nf.p (marked as nf in b). Two nuclei within one cell indicated the mitosis process (marked as * in b). Scale bar: 50μm.

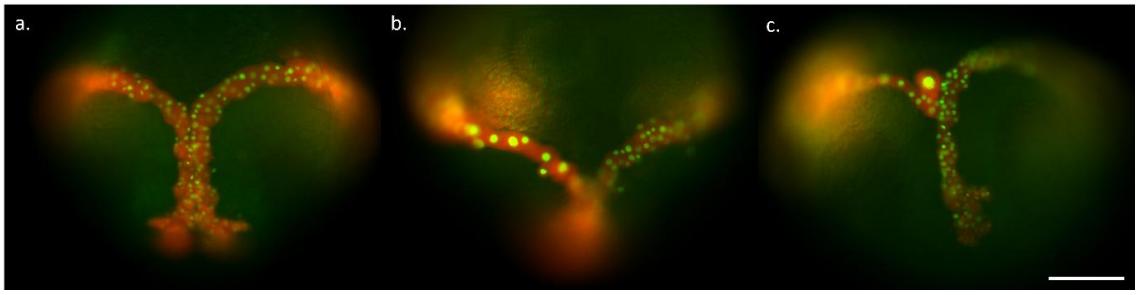

Figure 6. The effects of over-injection in single N teloblasts at 90 hpi. In embryo injected by an optimal dose, two N bandlets fused at ventral midline at this stage (a). One-sided over injection in left N teloblasts caused abnormal division of blast cells and misalignment of two N bandlet (b, c). Anterior is positioned to the bottom. Scale bar: 100μm.

doi:10.6342/NTU202502160

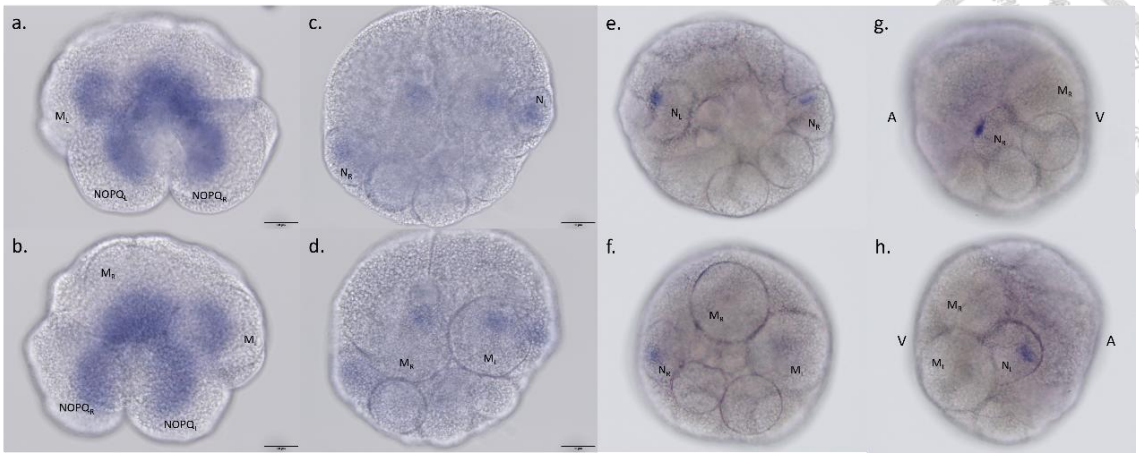

Figure 7. *In situ* hybridization of EST-based gene *Hau-EGL13a*. (a, b) Stage 5 embryos, with (a) viewed from the animal pole and (b) from the vegetal pole. (c, d) Stage 7 embryos at different focal planes: (c) focuses on the N teloblasts, while (d) focuses on the M teloblasts. (e–h) Stage e8 embryos: (e) viewed from the animal pole, (f) from the vegetal pole, and (g, h) from the lateral side. In (g, h), "A" indicates the animal pole and "V" indicates the vegetal pole. At stage 5, *Hau-EGL13a* is expressed in the M teloblasts and in the proteloblasts NOPQ. At stage 7, signals are present only in the M and N teloblasts. By stage e8, distinct signals are detected exclusively in the N teloblasts. Scale bar: 50μm.

doi:10.6342/NTU202502160

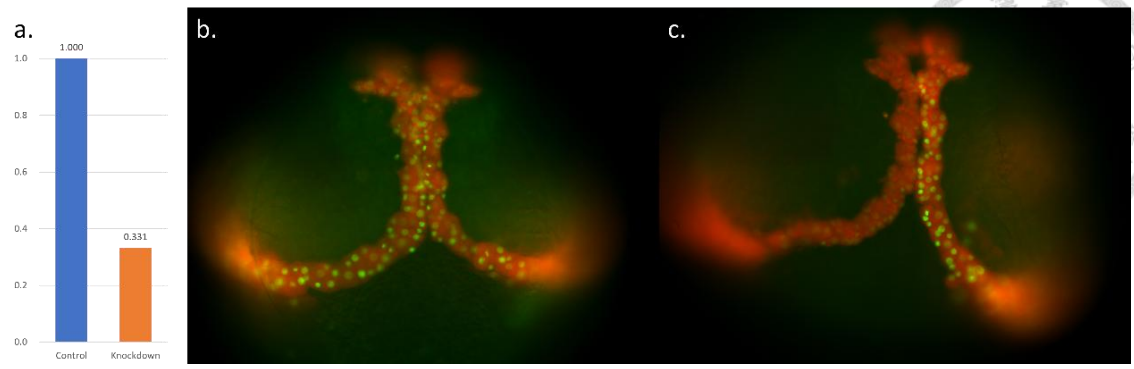

Figure 8. *Hau-EGL13a* knockdown using Cas13d. (a) Quantitative PCR (qPCR) results of *Hau-EGL13a* knockdown. Embryos from a single batch were divided equally: one half served as the control group, while the other half was injected with Cas13d mRNA and *Hau-EGL13a* guide RNA into the D' macromere at stage 4a. qPCR was performed three days post-injection. The mRNA level in the control group was normalized to 1; the normalized mRNA level in the knockdown group was 0.331. (b) Control phenotype of N bandlets. (c) Knockdown phenotype. In panel (c), the left side was injected with Cas13d mRNA and GFP guide RNA as a negative control, while the right side received Cas13d and *Hau-EGL13a* guide RNA. RDX (a cytoplasmic tracer emitting red fluorescence) and H2B:GFP (a nuclear tracer emitting green fluorescence) were co-injected as markers. Comparing (b) and (c), the co-injection of Cas13d mRNA and GFP guide RNA reduced green fluorescence in the left bandlet but did not affect its development. Likewise, co-injection of Cas13d and *Hau-EGL13a* guide RNA did not induce any observable phenotypic change.

doi:10.6342/NTU202502160

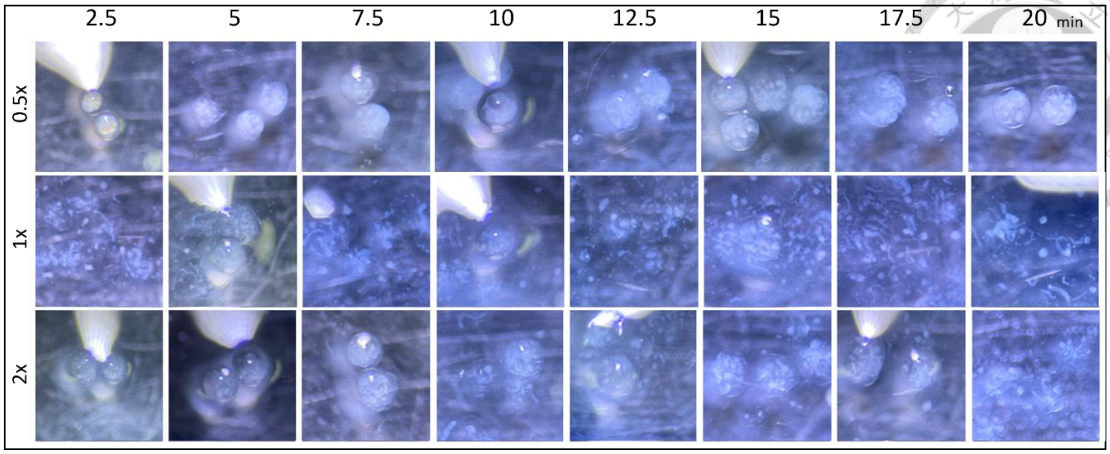

Figure 9. ACME treatment. Thirty stage-8 embryos were treated with 0.5×, 1×, and 2× ACME. A small drop containing ACME-treated embryos was collected every 2.5 minutes for imaging. Treatment with 0.5× ACME preserved embryo integrity, though cell junctions were slightly loosened. Embryos treated with 1× ACME dissociated into isolated teloblasts and partially separated bandlets within 2.5 minutes. Treatment with 2× ACME resulted in embryo dissociation while maintaining the integrity of the vitelline membranes.

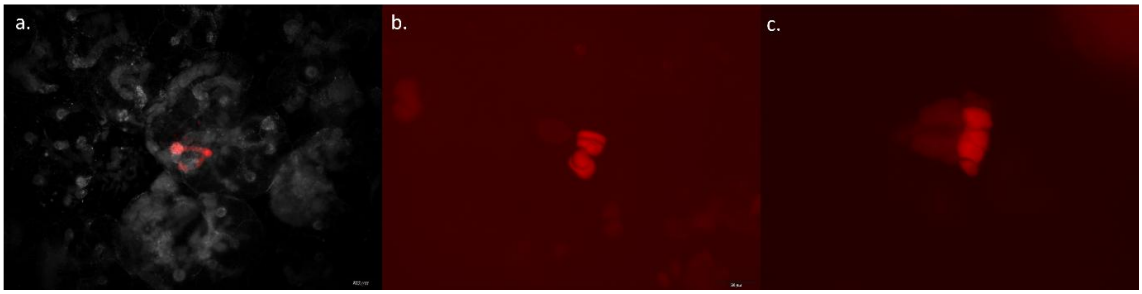

Figure 10. ACME treatment on fluorescence labeled embryos. Embryos were labeled by injecting RDX into the N teloblast at stage 6a and subsequently treated with 1× ACME at stage 8. (a) The labeled N bandlet is clearly distinguishable from non-labeled cells. (b, c) ACME treatment did not fully dissociate the bandlet.

doi:10.6342/NTU202502160

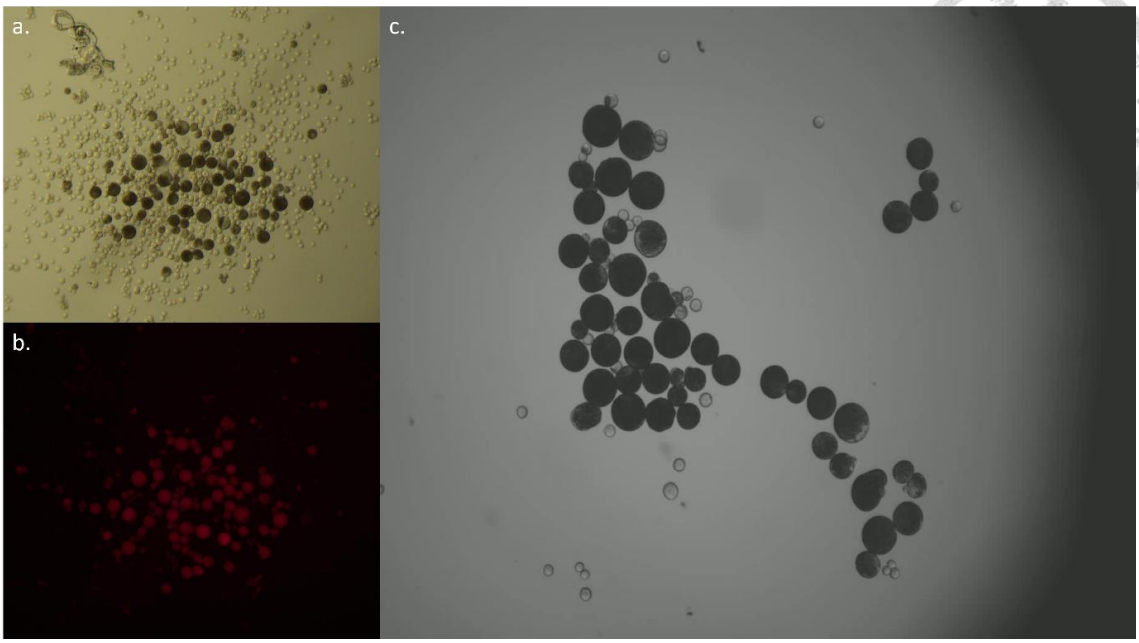

Figure 11. DTT/Trypsin Solution Treatment on Fluorescence-Labeled Embryos. Embryos were labeled by injecting RDX into the N teloblast at stage 6a and subsequently treated with DTT/trypsin solution at stage 7. The treatment successfully isolated N teloblasts, as observed in bright field (a) and fluorescence channel (b). (c) The isolated teloblasts ceased cell division.

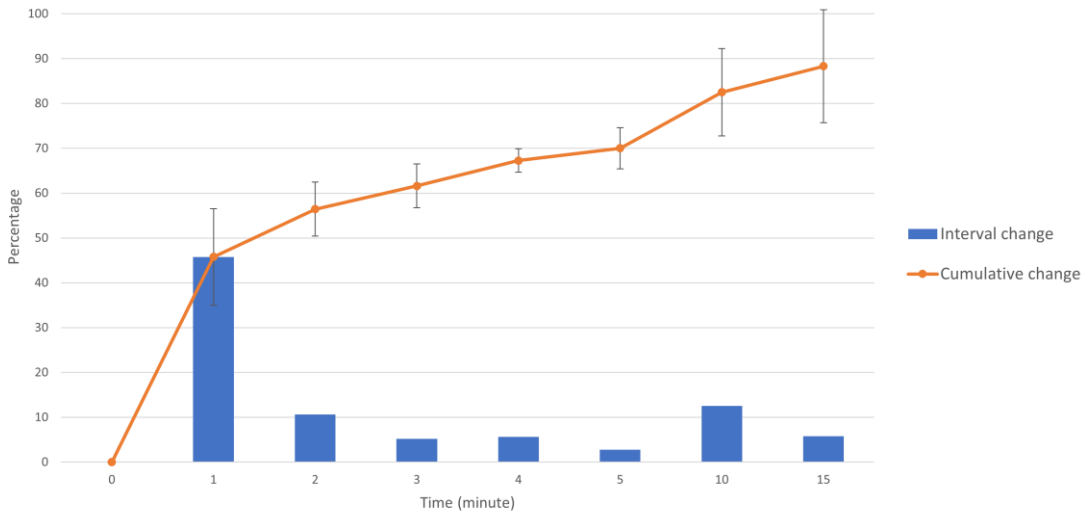

Figure 12. DTT/Trypsin Solution Devitellinization Rate. DTT/trypsin solution exhibits the highest enzymatic activity within the first minute, with the devitellinization rate decreasing over time.

doi:10.6342/NTU202502160

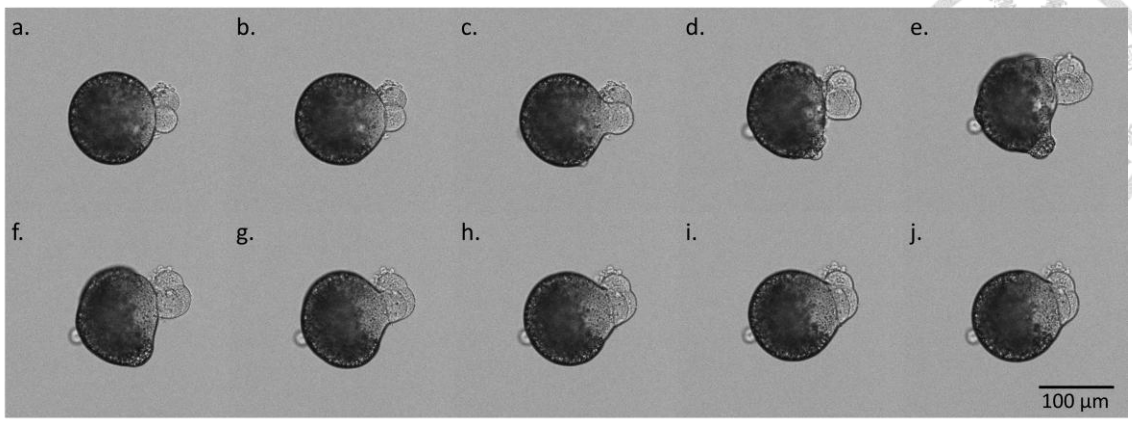

Figure 13. Time-lapse images of asymmetric cell division by an isolated N teloblast. (a, b) The isolated N teloblast undergoes independent division, initiating a budding extension. (c) The connection between the teloblast cell body and the budding extension contracts to form a bulb-like structure. (d-f) The bulb-like structure separated from the teloblast cell body, completing the asymmetric cleavage and resulting in two unequally sized daughter cells. (g-j) The teloblast gradually reverts to its spherical shape. Frames (a-j) were captured every 5 minutes in chronological order. Scale bar: 100µm.

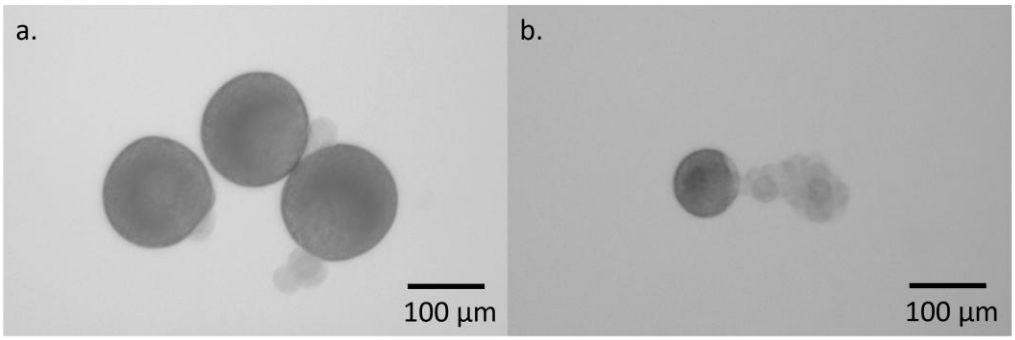

Figure 14. The isolated N teloblast maintains the cleavage axis. All cleavage events originated from a specific position of the teloblasts from 5 hour-post-surgery (hps) (a) to 24 hps (b). The new born blast cell pushed the elder cells away from the teloblast, forming a band-like structure. Scale bar: 100µm.

doi:10.6342/NTU202502160

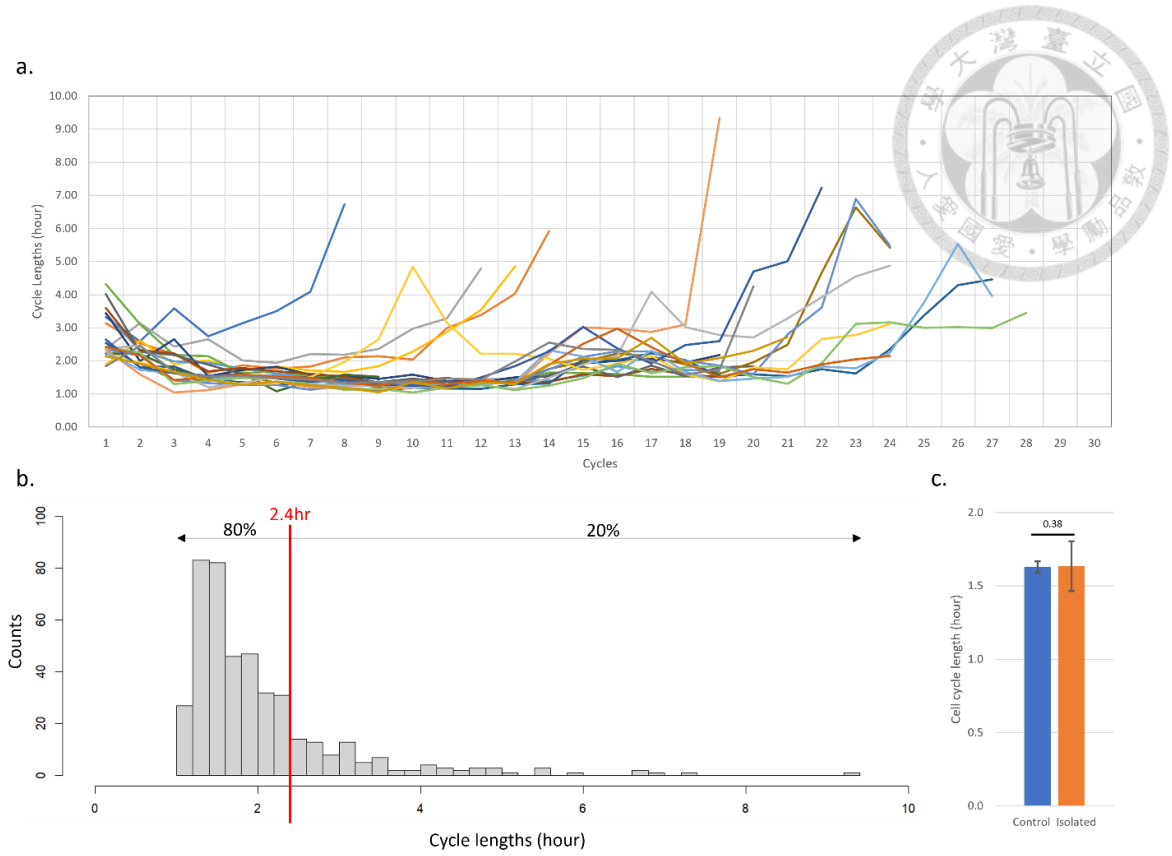

Figure 15. Cell cycles in isolated N teloblasts. (a) Cell cycle length across successive cycles, with each line representing an individual isolated teloblast. All teloblasts were monitored until their cell cycles ceased. (b) Distribution of cell cycle lengths, where 80% of cycles are under 2.41 hours, with the most enriched interval between 1.4–1.6 hours. (c) Comparison of cell cycle lengths between N teloblasts in embryos (control) and isolated N teloblasts (isolated). The average cycle lengths are 1.63 and 1.67 hours for control and isolated groups, respectively. The p-value of 0.38 indicates no significant difference between the two conditions.

doi:10.6342/NTU202502160

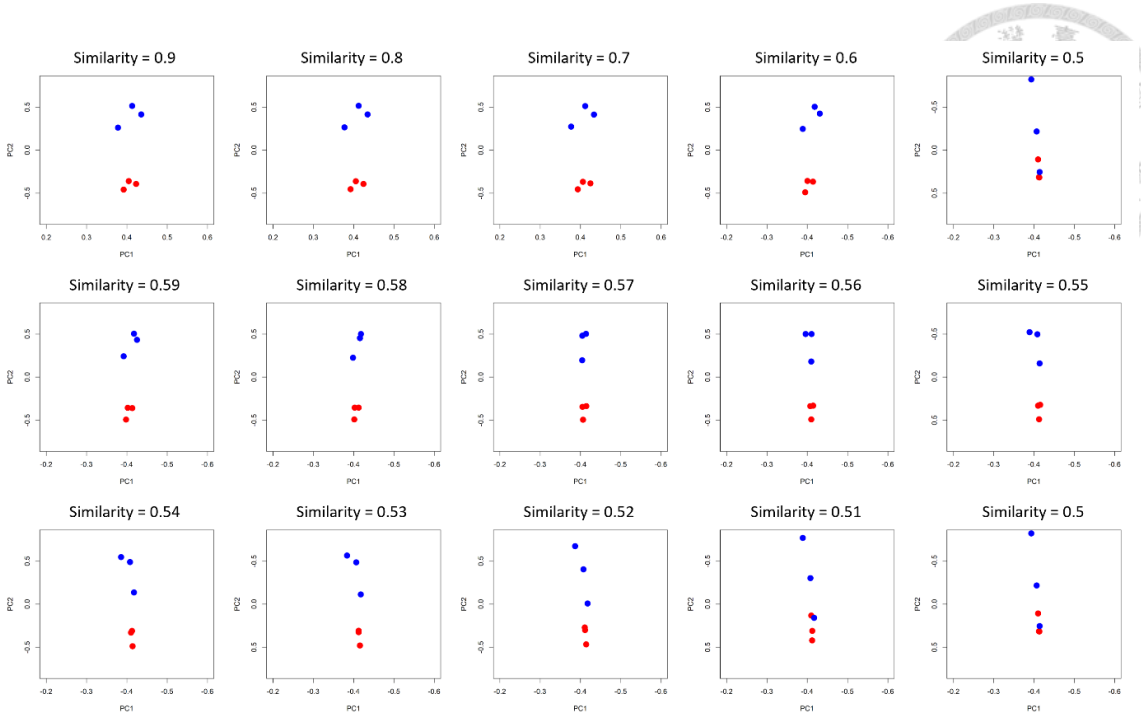

Figure 16. Principal Components Analysis of CD-HIT Clustered Data. The CD-HIT clustering was performed through a sequential adjustment of the parameter "similarity". As the similarity threshold decreased, variability along PC1 was reduced, while the separation along PC2 increased. Blue dots represent the isolated N teloblasts, while red dots represent whole embryos.

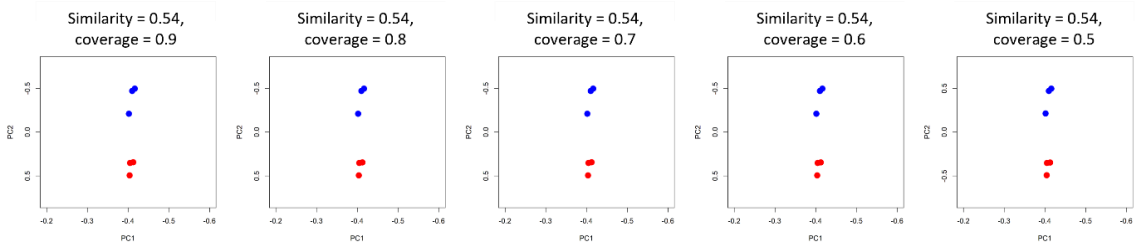

Figure 17. The impact of adjusting the coverage threshold in CD-HIT clustering. Clustering was performed at a fixed similarity of 0.54, with the coverage threshold gradually reduced from 0.9 to 0.5. Blue dots represent the isolated N teloblasts, while red dots represent whole embryos.

doi:10.6342/NTU202502160

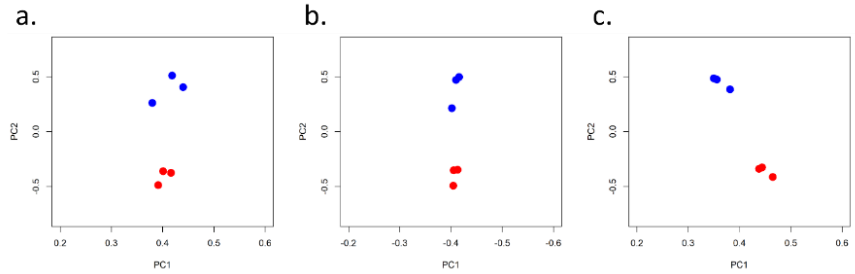

Figure 18. Comparison of raw, CD-HIT clustered, and Hro-annotated datasets. (a) shows the PCA of the raw dataset, (b) represents the CD-HIT clustered dataset, and (c) depicts the Hro-annotated dataset. Blue dots represent isolated N teloblasts, while red dots represent whole embryos. Compared to (a), (b) and (c) exhibit shorter distances among the isolated N teloblast data points, suggesting reduced redundancy.

doi:10.6342/NTU202502160

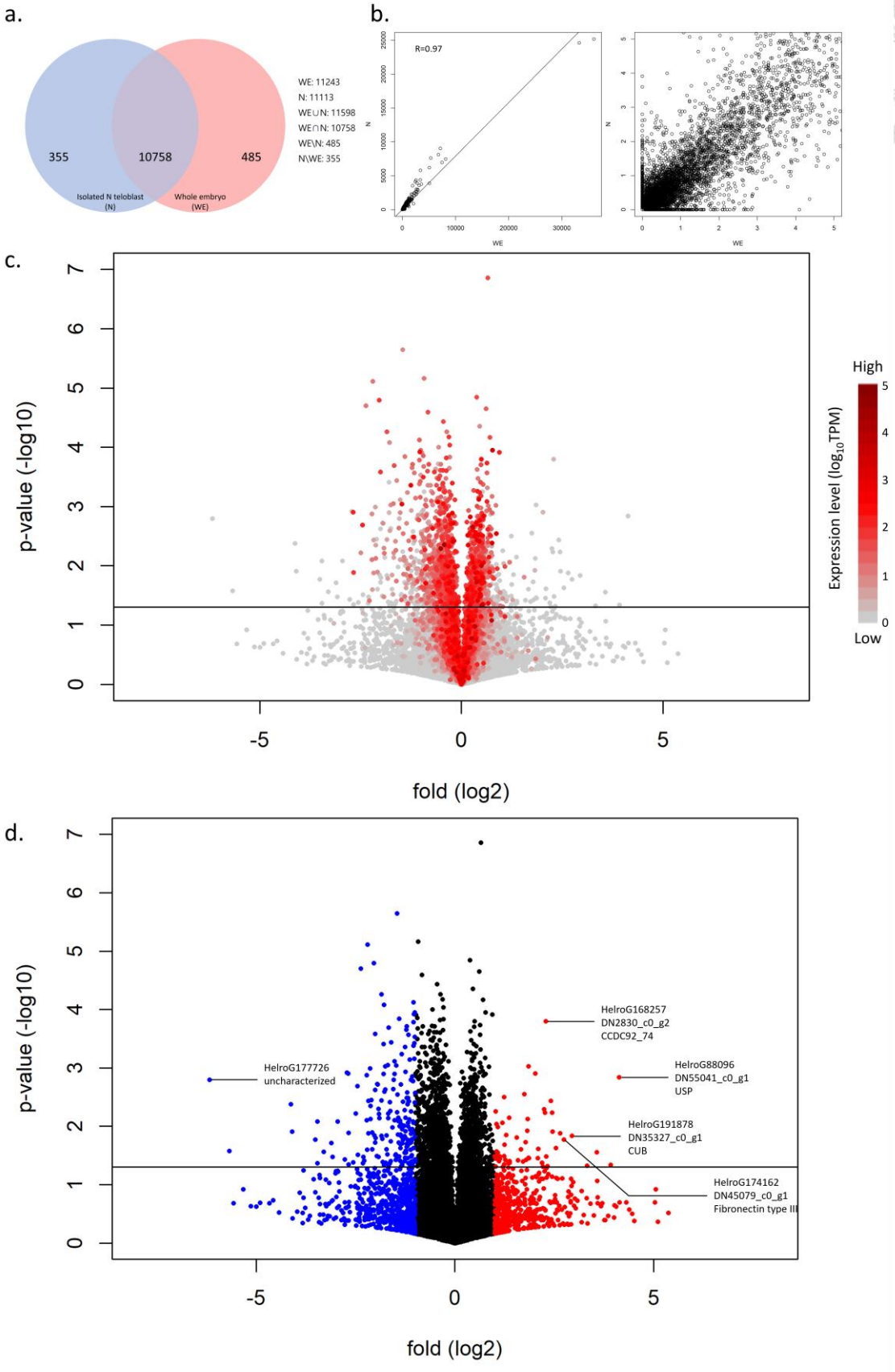

doi:10.6342/NTU202502160

Figure 19. Differentially expressed genes analysis between whole embryos (WE) and isolated N teloblasts (N). (a) A Venn diagram of the DEG analysis result. There are 11598 annotated genes in the Hro annotated dataset, with 11,243 detected in whole embryos (WE) and 11,113 detected in isolated N teloblasts (N). (b) Highly expressed genes generally showed no differential expression between WE and N, while the differentially expressed genes had low expression level. (c) A volcano plot of the DEG analysis. The most significantly N-enriched gene is HelroG88096, a USP containing domain protein. The genes significantly enriched in both Hro annotated dataset and CD-HIT clustered dataset are HelroG168257, HelroG191878 and HelroG174162, which encode CCDC92_74 protein, CUB domain containing protein and fibronectin type III. The most significantly N-deficient gene is HelroG177726, which is uncharacterized. (d) Most of differentially expressed genes exhibit low expression level.

doi:10.6342/NTU202502160

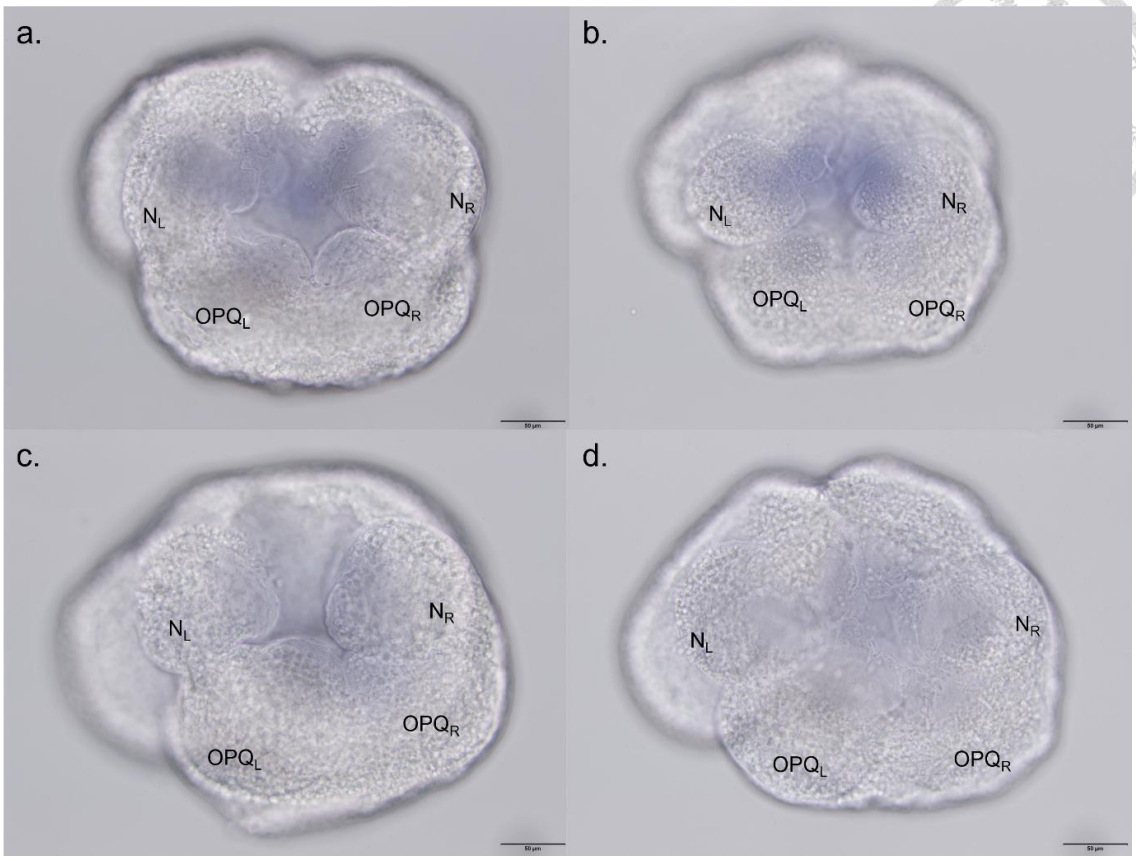

Figure 20. *In situ* hybridization of N-enriched genes. *In situ* hybridization of HelroG88096 (a), HelroG168257 (b), HelroG191878 (c), and HelroG174162 (d), all viewed from the animal pole. The color reaction was halted upon the appearance of background noise. In all conditions, in situ hybridization signals are expressed in teloplasm and the inner surface of blastocoel.

doi:10.6342/NTU202502160

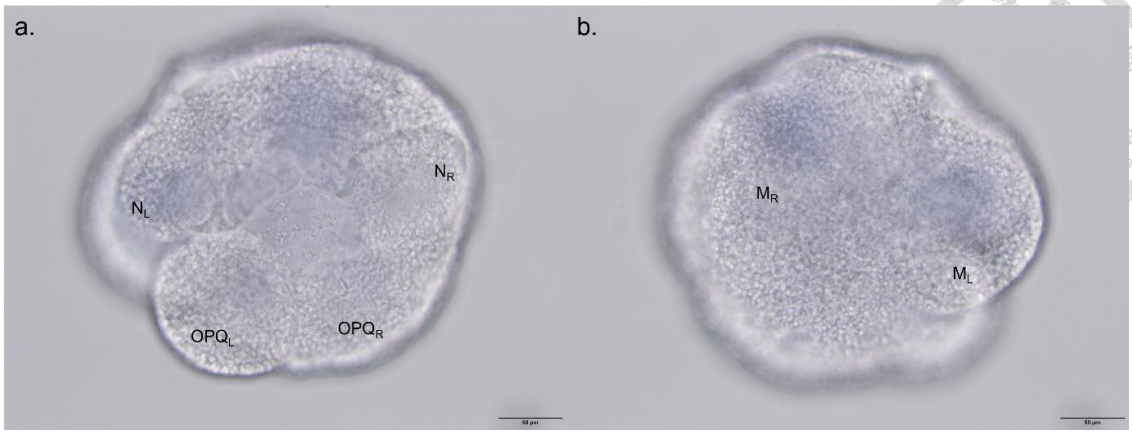

Figure 21. *In situ* hybridization of N-deficient HelroG177726. (a) is viewed from animal pole while (b) is viewed from vegetal pole. M teloblasts exhibit the strongest signals, whereas N teloblasts show almost no signal. Note that in (a), the signal originates from M_L and is observed through the transparent N_L, rather than originating from N_L itself.

doi:10.6342/NTU202502160

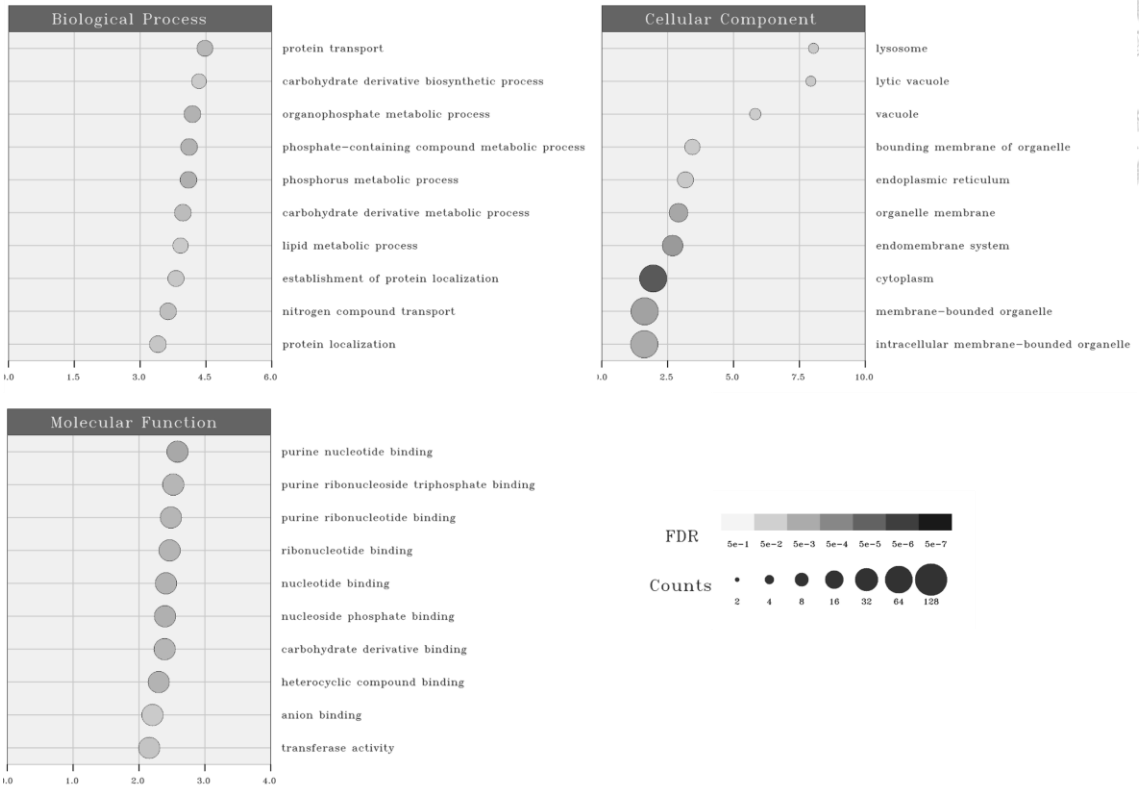

Figure 22. GO analysis of N-enriched genes. The N-enriched gene were selected based on a p-value less than 0.05 and a log2 fold change greater than 0.585 ($\log_2$ 1.5). The x-axis represents the enrichment score, dot size indicates the number of genes associated with each GO term, and dot color reflects statistical significance. All terms are arranged by the scores.

doi:10.6342/NTU202502160

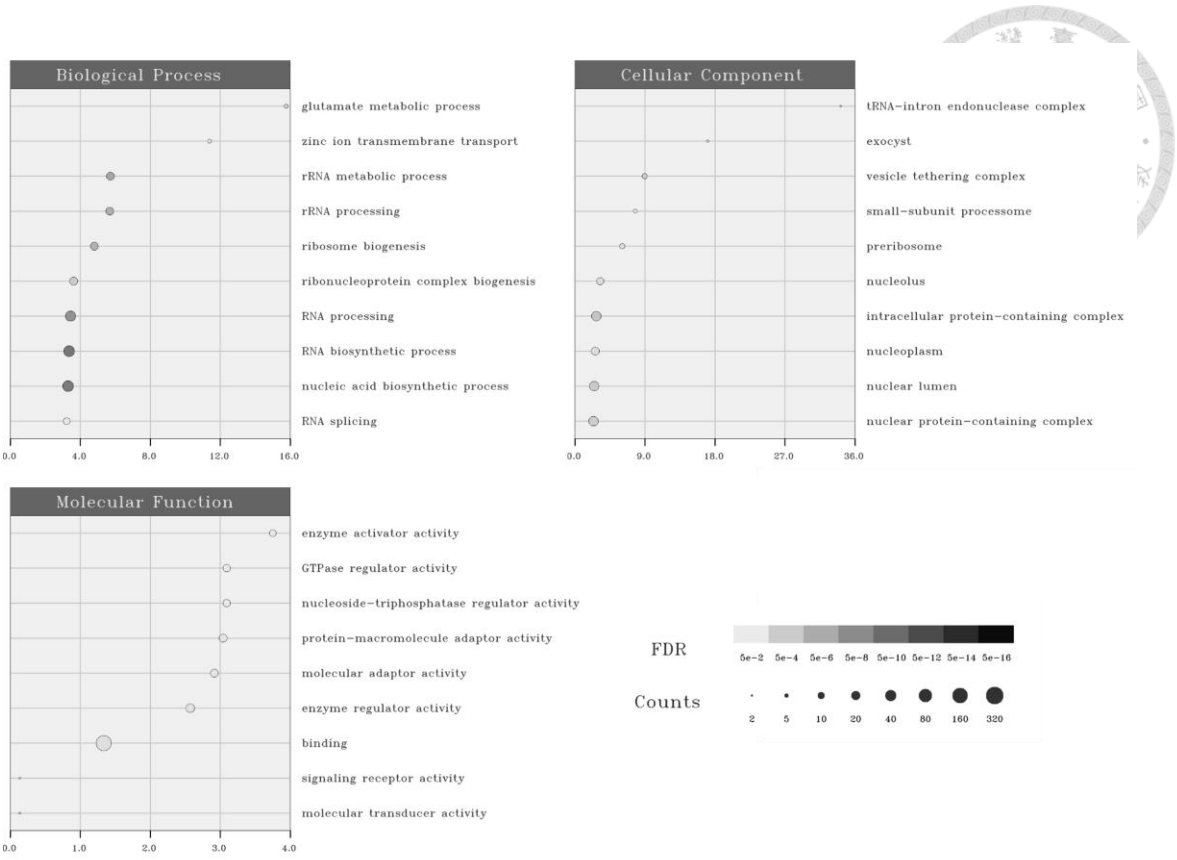

Figure 23. GO analysis of N-deficient genes. The N-deficient gene were selected based on a p-value less than 0.05 and a log2 fold change less than -0.585 ($-\log_2 1.5$). The x-axis represents the enrichment score, dot size indicates the number of genes associated with each GO term, and dot color reflects statistical significance. All terms are arranged by the scores.

doi:10.6342/NTU202502160